

In Situ Reprogrammings of Splenic CD11b⁺ Cells by Nano-Hypoxia to Promote Inflamed Damage Site-Specific Angiogenesis

주저자 논문, Author Contributions에 표기되어 있음.

Seyong Chung, Si Yeong Kim, **Kyubae Lee**, Sewoom Baek, Hyun-Su Ha, Dae-Hyun Kim, Suji Park, Chan Hee Lee, Hye-Seon Kim, Young Min Shin, Seung Eun Yu,* and Hak-Joon Sung*

Clinical translation of nanoparticles is limited because of their short circulation time, which hampers targeting to prolong therapeutic effects. Angiogenesis is required to regenerate damaged sites under inflammation, and CD11b⁺ cells turn vasculogenic under hypoxia. As a turning-point strategy to increase the circulation time, this study explores liposomal targeting of splenic CD11b⁺ cells, which are gathered in the spleen and move to inflamed sites inherently. Moreover, nano-hypoxia is strategized as a therapeutic method by loading liposomes with a hypoxic-mimetic agent (CoCl₂) to induce in situ reprogramming of splenic CD11b⁺ cells upon venous injection. Consequently, the vasculogenic potential of reprogrammed cells accelerates regeneration through inflammation-responsive homing. Hydrophilic coating of liposomes improves the selectivity of splenic targeting in contrast to fast targeting without coating. Hypoxia chambers and surgical induction of splenic hypoxia are compared to validate the reprogramming effect. The strategy is validated in mouse models of inflamed skin, ischemic hindlimbs, and 70% hepatectomy compared with a conventional approach using bone marrow cells. Intravital multiphoton microscopy, ¹⁹F 2D/3D MRI, and microchannel hydrogel chips for 3D tissue culture are used as advanced tools. Overall, nanocarrier change to CD11b⁺ cells prolong targeting by inducing in situ reprogramming for inflammation-responsive vasculogenic therapy.

limited duration of nanoparticle circulation in the body has been a long-standing unmet need, regardless of nanoparticle design for clinical applications. This hurdle hampers prolonged targeting to produce sufficient therapeutic effects, as nanoparticles are spontaneously cleared by absorptive organs, such as the spleen and liver, and this process is accelerated by protein adsorption and cellular uptake.

Another design point to improve for successful translation is accurate targeting, so that the therapeutic effect can be concentrated at the target site while avoiding systemic side effects. As a common approach, molecular binding-based targeting poses a risk because a unique molecular zip code is rare throughout the body and overlapping events of molecular expression often occur in unforeseen cases of pathogenesis. Finally, because the pathogenic events are spatiotemporally sporadic and often repeated, targeting a specific site at a given time must be strategized. Although therapeutic release can be programmed in response to abnormal

pathological stimuli, such as temperature, pH, and reactive oxygen species, precise control of release is impossible because of case-dependent variations in the degree and type of stimuli, in addition to systemic overlapping of these variations.

Hence, with a change in thinking, a clearance organ can be reverted to a reservoir of second cell carriers to prolong the delivery effect of the first nanocarriers after systemic injection. Next, the second cell carrier can be reprogrammed in situ to enable stimulus-responsive targeting and therapy through the reprogrammed functions. CD11b⁺ cells are identified as primarily monocytes with expression of the pan-myeloid marker (CD11b) and uptakes nanoparticles in the spleen, and the spleen is focused as a reservoir of CD11b⁺ cells because the spleen allows CD11b⁺ cells to enter from the blood circulation and to leave into inflamed sites.^[1–4] Although other clearance organs (e.g., liver, kidney, lung, and gastrointestinal tract) also filter up nanoparticles from the blood circulation of body, it remains unclear when and how CD11b⁺ cells to leave these organs back

1. Introduction

Continuous progress has been made in the development of nanoparticles as promising theranostic tools. However, the

S. Chung, S. Y. Kim, K. Lee, S. Baek, H.-S. Ha, S. Park, C. H. Lee, H.-S. Kim, Y. M. Shin, S. E. Yu, H.-J. Sung
Department of Medical Engineering
Yonsei University College of Medicine
Seoul 03722, Republic of Korea
E-mail: seungeunyu@yuhs.ac; hj72sung@yuhs.ac

D.-H. Kim
Department of Veterinary Surgery
College of Veterinary Medicine
Chungnam National University
Daejeon 34134, Republic of Korea

 The ORCID identification number(s) for the author(s) of this article can be found under <https://doi.org/10.1002/adfm.202302817>.

DOI: 10.1002/adfm.202302817

into the circulation toward inflamed sites. Hence, the clearance of circulating liposomes by the spleen with CD11b⁺ cell uptake is strategized as a means of splenotropic targeting.^[5,6] Inflammation occurs as a result of tissue damage and ischemia, and CD11b⁺ cells spontaneously migrate to inflamed sites.^[1,4,7,8] The reversal of splenic CD11b⁺ cells to the second carriers of cargo delivered by liposomes (“carrier change”) can provide an impactful advantage by utilizing the inherent homing ability of these cells to the inflamed sites.

As a therapeutic aspect, CD11b⁺ cells may serve as a therapeutic option for vascular diseases.^[9–12] However, clinical trials have exhibited only marginal therapeutic efficacy,^[13,14] and the small number of CD11b⁺ cells obtained upon extraction has been suggested as a possible limitation.^[15,16] In addition, previous clinical studies used invasive angiography for vasculogenic cell delivery to ischemic sites,^[13,14] which is associated with the risk of hemorrhage and thrombosis. CD11b⁺ cells undergo vasculogenic differentiation under hypoxia,^[17–20] which relies on the expression and stabilization of hypoxia-inducible factor (HIF)-1 α .^[17–22] Hence, splenic CD11b⁺ cells are a promising option to overcome the shortcomings above. The spleen is enriched with CD11b⁺ cells that can attain vasculogenic potential by inducing hypoxia and spontaneously targeting the damage sites in an inflammation-responsive manner.

The present study looked at nano-hypoxia as a turning point strategy from conventional nanoparticle-based approaches toward successful translation. This new strategy utilizes splenotropic targeting of liposomes as the first carrier, so that splenic CD11b⁺ cells can take over the delivery of cargo that liposomes carry following the concept of carrier change. Liposomes were loaded with a hypoxic mimetic agent (CoCl₂), which was introduced into the mouse tail vein, so that splenic CD11b⁺ cells undergo vasculogenic differentiation upon intracellular uptake of CoCl₂-liposomes (“in situ reprogramming”). CoCl₂ treatment has been confirmed to promote the expression and stabilization of HIF-1 α , with consequent vasculogenic reprogramming of splenic CD11b⁺ cells^[18] as a hypoxic mimetic agent.^[23] After reprogramming, the vasculogenic cells exhibit inflammation-responsive homing and subsequent proangiogenic functions. A series of experimental models were employed, including in vitro co-culture with endothelial cells under inflammation induction, ex vivo 3D cultures of normal and inflamed tissues on a micro-channelized hydrogel chip, and in vivo mouse models of inflamed skin, hindlimb ischemia (+/– reperfusion), and partial hepatectomy. In particular, in vivo functions were observed using state-of-the-art imaging modalities, such as intravital multiphoton microscopy, ¹⁹F 2D/3D magnetic resonance imaging (MRI), and in vivo imaging system (IVIS). The nano-hypoxia effects were validated by comparison with the hypoxia chamber, surgical induction of splenic hypoxia, and conventional approaches using bone marrow (BM) cells.

2. Results

2.1. Liposomal Targeting to Splenic CD11b⁺ Cells

As liposomes spontaneously target the spleen, where CD11b⁺ cells accumulate and naturally move to inflamed sites, this

circulatory mechanism was applied to propose two “carrier change” strategies (Figure 1a). i) CD11b⁺ cells were used as second carriers of cargo delivered by liposomes. ii) CD11b⁺ cells were reprogrammed to vasculogenic cells by inducing hypoxia through liposomal targeting with the delivery of a hypoxic-mimetic agent (“nano-hypoxia”). As the first step to establishing the two strategies, liposomes were produced with average sizes of 119 and 127 nm, respectively, without and with a hydrophilic coating, under the formation of typical circular shapes (range: 100–150 nm), as confirmed by transmission electron microscopy (TEM) (Figure S1a, Supporting Information). Liposomes were injected through the tail vein of mice after either being tagged with DiD or loaded with gold nanoparticles as a type of cargo (Figure 1b).

Red pulp of the spleen is the site where CD11b⁺ cells are gathered,^[1] and intense colocalization signals were noted between CD11b⁺ cells (red, CD11b) and coating (–) liposomes (green, DiD) at 12 h after tail vein injection (Figure 1c; Figure S1b, Supporting Information). When monocytes were separated from other splenocytes as the major population of splenic CD11b⁺ cells, this result was further supported by liposomal accumulation (red, DiD) inside the CD11b⁺ cell (green, wheat germ agglutinin) after 12 h (Figure 1d). These observations were confirmed by coating (+) liposomes, as evidenced by the maintenance of the higher range in radiant intensity (3–15 $\times 10^6$, CD11b⁺) for 72 h compared with that in other splenocytes (CD11b[–]) (Figure 1e; Figure S1c, Supporting Information). As a proof of concept for cargo delivery, gold nanoparticles (diameter = 5 nm) were loaded into coating (+) liposomes, and subsequent delivery to splenic CD11b⁺ cells for 72 h was identified using TEM (Figure 1f). Upon zoom observation (Figure S1d, Supporting Information), gold signals appeared clearly in a monocyte, as identified based on the 2:1 ratio of nucleus to cytoplasm.

2.2. Hydrophilic Coating Effects on Liposomal Targeting

Hydrophilic coating of liposomes with polyethylene glycol (PEG) increases circulation time by suppressing protein adsorption. Hence, the coating effects on the speed and selectivity of splenic targeting were examined through tail vein injection of DiD-tagged liposomes from 0–2 min to 0.5–72 h using intravital multi-photon microscopy, IVIS, and confocal microscopy (Figure 1g). For intravital microscopic evaluation at 0–2 min post-liposomal injection (Figure S2a, Supporting Information), each mouse was anesthetized with an abdominal incision. The spleen was closely exposed to the lens, followed by tail vein injection of liposomes. Intravital microscopic imaging revealed that the coating (–) liposomes (red, DiD) accumulated in splenic CD11b⁺ cells (green, CD11b) over 10-fold faster for 50 s than the coating (+) liposomes (0.0035 vs. 0.0003), (Figure 1h) as confirmed by IVIS during 0.5–6 h (Figure S2b, Supporting Information).

This high-speed targeting of coating (–) liposomes (1-fold) to splenic CD11b⁺ cells from blood circulation was dominant for the initial 12 h, as confirmed using IVIS with quantitative analysis and confocal imaging analysis (Figure 1i; Figure S2c, Supporting Information). In contrast, coating (+) liposomes started

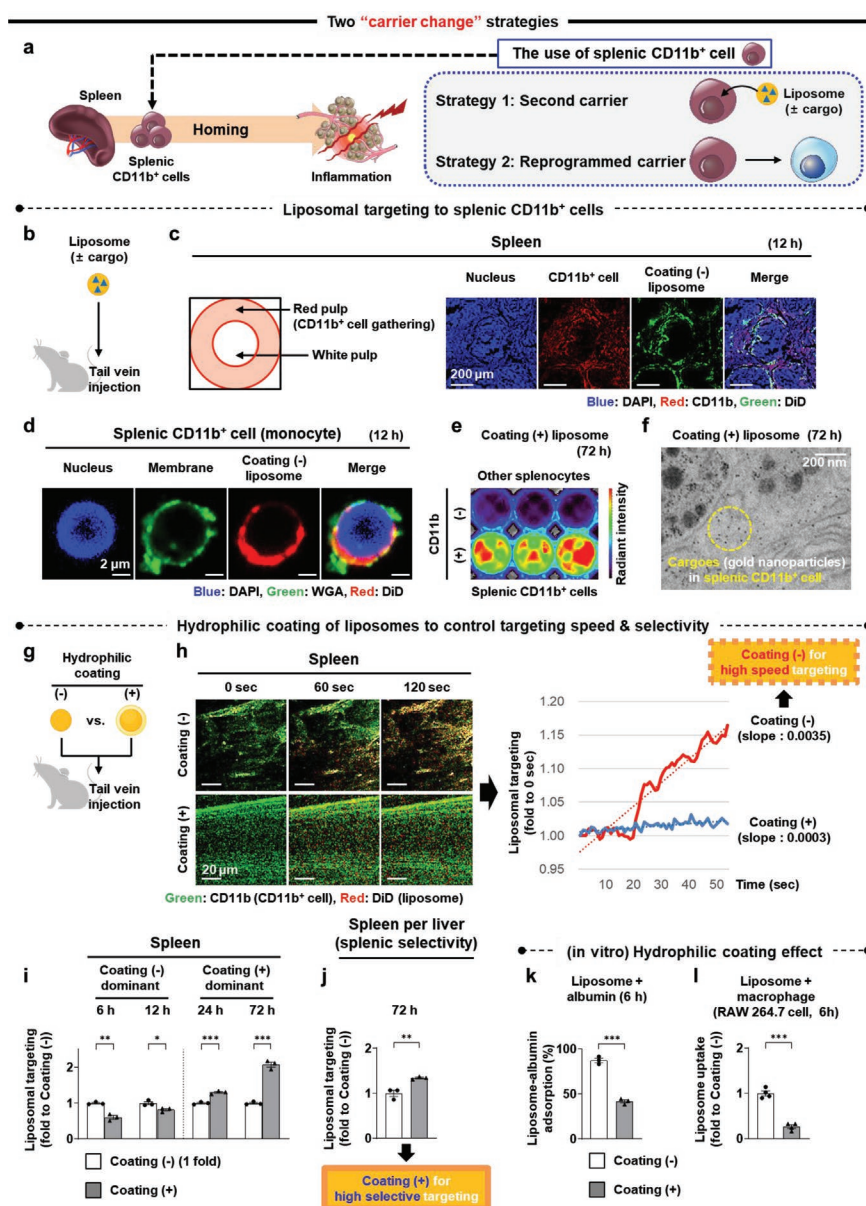


Figure 1. Characterization of liposomal targeting to splenic CD11b⁺ cells as a programmable carrier for inflammation-responsive homing. **a**) As liposomes spontaneously targets the spleen, where CD11b⁺ cells accumulate and naturally move to inflamed sites, this circulatory mechanism was applied to propose two "carrier change" strategies. **i**) CD11b⁺ cells were used as second carriers of cargo delivered by liposomes. **ii**) CD11b⁺ cells were reprogrammed to vasculogenic cells by inducing hypoxia through liposomal targeting with the delivery of a hypoxic-mimetic agent ("nano-hypoxia"). **b**) As the first step to establishing the two strategies, liposomes (+/- hydrophilic PEG coating) were injected through the tail vein of mice after either being tagged with DiD or loaded gold nanoparticles as the type of cargoes (N = 3). **c**) The red pulp of the spleen is the site where CD11b⁺ cells are gathered,^[1] and intense colocalization signals were noted between CD11b⁺ cells (red, CD11b) and coating (-) liposomes (green, DiD) at 12 h after tail vein injection. When monocytes were separated from other splenocytes as the major population of splenic CD11b⁺ cells, these results were further supported by **d**) liposomal accumulation (red, DiD) inside the CD11b⁺ cell (green, WGA) for 12 h. **e**) These results were confirmed in coating (+) liposomes, as evidenced by the maintenance of higher radiant intensity (3–15 × 10⁶) for 72 h in CD11b⁺ cells than in other splenocytes (CD11b⁻). **f**) As the proof of concept for cargo delivery, gold nanoparticles (diameter = 5 nm) were loaded into coating (+) liposomes, and subsequent delivery to splenic CD11b⁺ cells for 72 h was confirmed with transmission electron microscopy. **g**) As the hydrophilic coating of liposomes with PEG increases the circulation time by suppressing protein adsorption, the coating effects on the speed and selectivity of splenic targeting were examined in comparison with non-coating (-) after the tail vein injection of DiD-tagged liposomes (N = 3). **h**) Intravital multiphoton microscopic imaging revealed that the coating (-) liposomes (red, DiD) accumulated in splenic CD11b⁺ cells (green, CD11b) more than 10-fold faster than coating (+) liposomes did (0.0035 vs. 0.0003). **i**) While the observed high-speed targeting of coating (-) liposomes (1-fold) to splenic CD11b⁺ cells was dominant for 12 h, coating (+) liposomes started to accumulate in splenic CD11b⁺ cells dominantly more after 24 h and up to 2-fold for 72 h. **j**) Highly selective targeting by hydrophilic coating for a long period was further evidenced when the ratio of liposome accumulation in the spleen to the liver was compared between the coating (-) and (+) groups. As mechanistic insights with in vitro experiments, **k**) hydrophilic coating suppresses serum protein (albumin) adsorption (N = 3), **l**) with the consequent reduction in uptake by macrophages (RAW 264.7 cell) (N = 4), compared with non-coating (+) liposome in alignment with previous reports on splenotropic effects in hepatic Kupffer cells.^[5,6] (PEG: polyethylene glycol, WGA: wheat germ agglutinin) Data = mean ± SEM (N: dots on each graph). **p* < 0.05, ***p* < 0.01, and ****p* < 0.001 between lined groups.

to accumulate in splenic CD11b⁺ cells dominantly more after 24 h and up to 2-fold for 72 h (Figure 1i). High selective targeting by hydrophilic coating for a long period was further evidenced when the ratio of liposome accumulation in spleen to the liver was compared between the coating (–) and (+) groups (Figure 1j). High-speed targeting of coating (–) liposomes resulted in the loss of splenic selectivity, as evidenced by the faster accumulation of hepatic CD11b⁺ cells compared to the coating (+) liposomes upon IVIS and immunofluorescence staining analyses (Figure S2b and S2d, Supporting Information). Both types of liposomes were mainly distributed to the spleen and liver, while their distribution to the kidney was not significant during 6 h. In the IVIS analysis of the spleen and liver at 72 h, these two organs occupied over 80% of the liposomal targeting, regardless of the coating (Figure S2e, Supporting Information).

As mechanistic insights with in vitro experiments, hydrophilic coating suppressed serum protein (albumin) adsorption (Figure 1k) compared to non-coating. In addition, coating (–) and (+) liposomes were compared by incubation with albumin solution for 6 h (Figure S3a, Supporting Information). Albumin without liposomal adsorption (peak below 10 nm) was analyzed by separating it from liposome +/- albumin (peak above 10 nm) with dynamic light scattering. Consequently, the coating significantly increased the amount of absorption-free albumin, thereby validating the anti-fouling effect. Furthermore, the effect of the coating on the suppression of macrophage uptake was examined by incubating coating (–) and (+) liposomes with macrophages (RAW 264.7 cells) for 6 h without or with inflammatory induction by lipopolysaccharide (LPS) treatment (Figure S3b, Supporting Information). The coating substantially reduced liposomal uptake by macrophages compared with non-coating even without LPS treatment (Figure 1l; Figure S3c, Supporting Information), and this reduction was more evident following LPS treatment (Figure S3d, Supporting Information). These results are consistent with previous reports on splenotropic effects using hepatic Kupffer cells.^[5,6]

When nanovesicles were produced using human tonsil-derived mesenchymal stem cells (TMSCs) with or without hydrophilic coating, coating (–) nanovesicles exhibited high-speed targeting to the spleen at 3 h compared with a coating (+) nanovesicles in IVIS with quantitative analysis (Figure S3e, Supporting Information). These results confirmed that the hydrophilic coating effect is not specific to liposomes and applies to other types of nanoparticles.

2.3. Homing of Second Carrier to Inflamed Mouse Skin

Inflammation degree-dependent homing of splenic CD11b⁺ cells was examined as the second carrier of liposomal delivery. As a homing site, skin inflammation was induced by subcutaneously implanting LPS-loaded gel into the back of mice for 7 days (Figure S4a, Supporting Information). The degree of inflammation was controlled by loading 0 (base), 20 (weak), or 120 µg (strong) LPS into the gelatin gel (d 0) for subcutaneous implantation, followed by tail vein injection of fluorescence-tagged coating (–) liposomes (d 1) and IVIS imaging (d 7) (Figure 2a). Because the inflammation was induced

before liposome injection, coating (–) was used to rely on high-speed targeting to the gel implantation site. The targeting was expected to accelerate immediately in response to LPS dose-dependent elevation of inflammation degree. As a model to repeat the inflammatory event at the same site, additional LPS induction was optionally performed (d 3) to increase the inflammatory severity with IVIS analysis before (d 2) and after (d 4). As the severity of inflammation increased from the base to a weak and further to a strong degree, cell invasion increased, as observed on day 7 using hematoxylin and eosin (H&E) staining, and the dominant portion of these cells was identified as CD11b⁺ cells (green, CD11b) on immunofluorescence staining (Figure S4b, Supporting Information).

In addition, the fluorescence intensity of coating (–) liposomes in the inflamed skin was increased as opposed to the decreased intensity in the spleen (radiant intensity range: $2.6\text{--}40 \times 10^8$) in the IVIS analysis (Figure 2b). The fluorescence intensity in the liver, as well as the combined intensity in the skin, spleen, and liver, remained unchanged. These findings suggest that coating (–) liposomes are transported from the spleen to the inflamed skin without affecting liver clearance or the total amount in circulation. The liposomal translocation to the inflamed skin was further supported by increased fluorescence intensity in inflamed skin (d 4) after the additional injection of LPS (d 3) compared with the intensity before the injection (d 2), as opposed to the decreased intensity in the spleen (radiant intensity range: $1.8\text{--}4 \times 10^7$) in IVIS analysis (Figure 2c). Since the spleen serves as a reservoir of CD11b⁺ cells that become the target of coating (–) liposomes upon tail vein injection, the number of CD11b⁺ cells (CD11b⁺) decreased in the spleen upon LPS induction in contrast to their increased number in the inflamed skin (Figure 2d), as confirmed by polymerase chain reaction (PCR) (Figure S4c, Supporting Information). When these cells were subjected to fluorescence-activated cell sorting (FACS), CD11b⁺ cells were identified as the more dominant carriers of coating (–) liposomes to the inflamed skin than CD11b[–] cells (Figure S4d, Supporting Information), consistent with the decremental and incremental trends of CD11b⁺ cells in the spleen and inflamed skin, respectively (Figure 2e).

2.4. CoCl₂ as A Programmer of Nano-Hypoxia

HIF- α undergoes degradation through hydroxylation by converting O₂ to CO₂ using Fe²⁺, which can be inhibited by hypoxia due to O₂ depletion and the consequent inhibition of HIF- α hydroxylation (Figure S5a, Supporting Information). Owing to its similar atomic number (AN = 27 vs. 26), Co²⁺ acts as a competitive inhibitor of Fe²⁺, thereby stabilizing HIF- α expression as a hypoxic-mimetic agent.^[23] The conventional approach requires invasive extraction of bone marrow cells with a series of out-body processes to facilitate angiogenesis (Figure 3a).^[10,11,13–15] In contrast, nano-hypoxia [CoCl₂-coating (+)] enables in situ reprogramming of splenic CD11b⁺ cells to promote vasculogenic potential through hypoxic priming by nano-size liposomes. Thus, nano-hypoxia provides clear advantages, including a non-invasive process, sufficient number of CD11b⁺ cells,^[1] and inflammation-responsive homing. Hypoxic priming by nano-hypoxia promotes the expression and

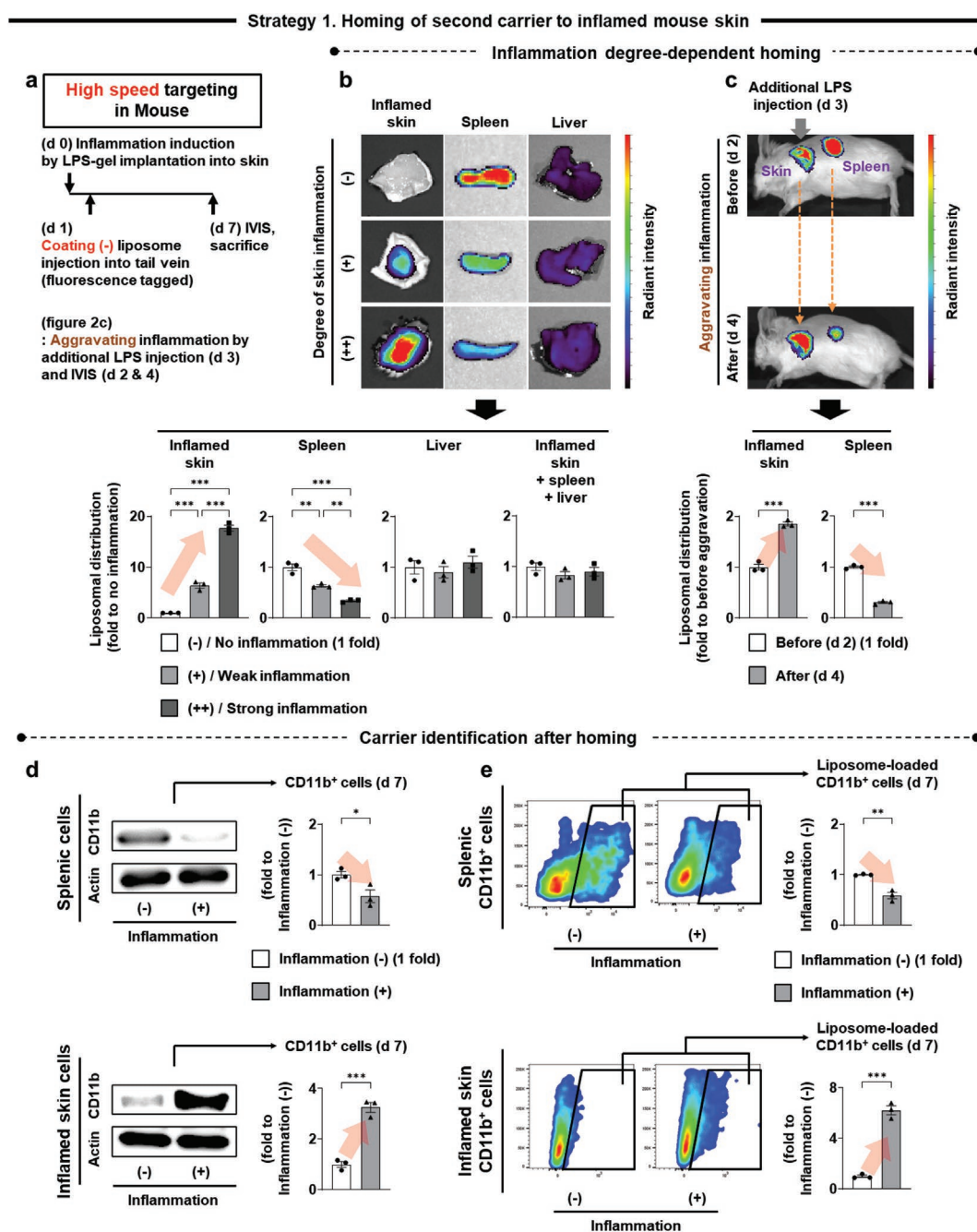


Figure 2. Inflammation degree-dependent homing of splenic CD11b⁺ cells as the second carriers for liposomal delivery. a) As the homing site, a mouse model of inflamed skin (N = 3) was established by subcutaneous implantation of an LPS-containing gel (d 0), followed by tail vein injection of fluorescence-tagged coating (-) liposomes (d 1) and IVIS analysis (d 7). Because the inflammation was induced before liposome injection, coating (-) was used to rely on high-speed targeting to the gel implantation site. The targeting was expected to accelerate immediately in response to LPS dose-dependent elevation of inflammation degree. As a model to repeat the inflammatory event at the same site (c), additional LPS induction was optionally performed (d 3) to increase the inflammatory severity with IVIS analysis before (d 2) and after (d 4). b) With the increase in the severity of inflammation, the fluorescence intensity of coating (-) liposomes in the inflamed skin was increased, as opposed to the decreased intensity in the spleen (radiant intensity range: $2.6\text{--}40 \times 10^8$) in the IVIS analysis. The fluorescence intensity in the liver, as well as the combined intensity in the skin, spleen, and liver, remained unchanged. These findings suggest that coating (-) liposomes are transported from the spleen to the inflamed skin without affecting liver clearance or the total amount in circulation. c) The liposomal translocation to the inflamed skin was further supported by increased fluorescence intensity in inflamed skin (d 4) after the additional injection of LPS (d 3) compared with the intensity before the injection (d 2), as opposed to the decreased intensity in the spleen (radiant intensity range: $1.8\text{--}4 \times 10^7$) in IVIS analysis. Since the spleen serves as a reservoir of CD11b⁺ cells that become the target of coating (-) liposomes upon tail vein injection, d) the number of CD11b⁺ cells decreased in the spleen upon LPS induction in contrast to their increased number in the inflamed skin. e) When these cells were sorted using FACS, a significant number of splenic CD11b⁺ cells were identified to carry the coating (-) liposomes, consistent with the decremental and incremental trends of CD11b⁺ in the spleen and inflamed skin, respectively. (LPS: lipopolysaccharide, IVIS: in vivo imaging system, FACS: fluorescence-activated cell sorting) Data = mean \pm SEM (N: dots on each graph). * $p < 0.05$, ** $p < 0.01$, and *** $p < 0.001$ between lined groups.

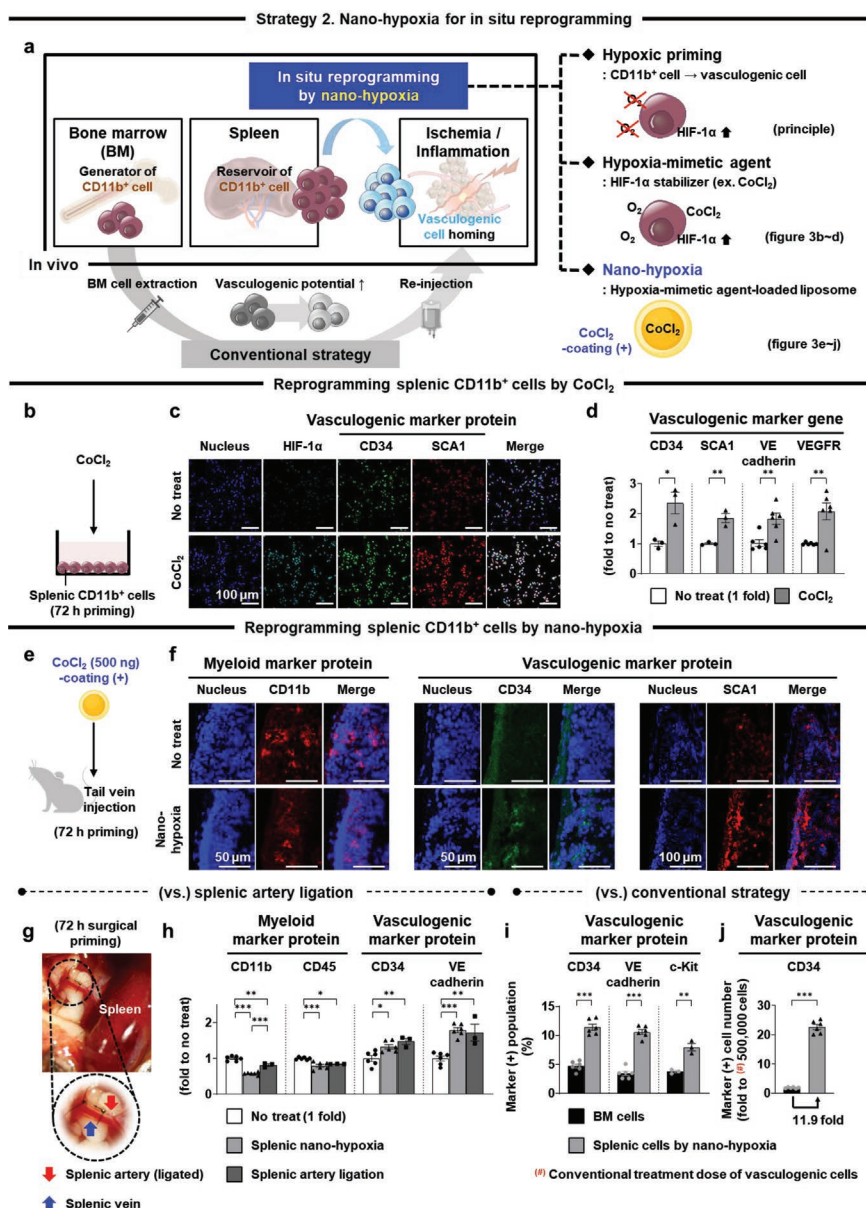


Figure 3. Validation of nano-hypoxia for in situ vasculogenic reprogramming of splenic CD11b⁺ cells. **a**) The conventional approach requires invasive extraction of BM cells with a series of out-body processes to facilitate angiogenesis.^[10,11,13–15] In contrast, nano-hypoxia [CoCl₂-coating (+)] enables in situ reprogramming of splenic CD11b⁺ cells to promote vasculogenic potential through hypoxic priming by nano-size liposomes. Thus, nano-hypoxia offers clear advantages, including non-invasiveness of the process, enough CD11b⁺ cells,^[1] and inflammation-responsive homing. Hypoxic priming by nano-hypoxia promotes the expression and stabilization of HIF-1α with consequent vasculogenic reprogramming of splenic CD11b⁺ cells.^[18] As CoCl₂ stabilizes HIF-1α expression as a hypoxic-mimetic agent,^[23] liposomes can deliver CoCl₂ into splenic CD11b⁺ cells, thereby inducing vasculogenic reprogramming upon hypoxic priming as a means of nano-hypoxia. **b**) The hypoxia-mimetic function of CoCl₂ was examined by treating splenic CD11b⁺ cells with priming for 72 h in vitro culture (N = 3–6). **c**) CoCl₂ treatment increased the protein expression of HIF-1α and vasculogenic markers (CD34 and SCA1) in splenic CD11b⁺ cells in immunofluorescence staining. **d**) These results were further supported by the gene expression of vasculogenic markers (CD34, SCA1, VE-cadherin, and VEGFR) by PCR,^[10,12] compared to the no treat group. **e**) Next, in vivo nano-hypoxia was induced by injecting CoCl₂ (500 ng)-coating (+) into the mouse tail vein for 72 h. **f**) As a result, the mouse spleen exhibited a significant reduction in the protein expression of the myeloid marker (CD11b), as opposed to that of vasculogenic marker proteins (CD34, SCA1), compared to the no treat group in immunofluorescence staining. These results indicate vasculogenic reprogramming of splenic CD11b⁺ cells by nano-hypoxia. **g**) This effect was compared with the surgical induction of hypoxia by ligating the splenic artery for 72 h (N = 3–6). **h**) Consistent with observations in the nano-hypoxia group, surgical induction of splenic hypoxia significantly reduced the protein expression of myeloid markers (CD11b and CD45) as opposed to that of vasculogenic markers (CD34 and VE-cadherin), compared to the no treat group in FACS. Nano-hypoxia was more effective than surgical induction in reducing the number of CD11b⁺ cells. Compared with BM cells after extraction from the femur (i.e., conventional approach), **i**) nano-hypoxia was superior in promoting the protein expression of vasculogenic markers (CD34, VE-cadherin, or c-Kit) in splenic cells. **j**) These results were further supported by comparison with the conventional treatment doses (500 000 cells) of vasculogenic cells^[9,10] because the number of CD34⁺ cells was up to 11.9 times higher in splenic nano-hypoxia compared to the BM cells (22.7 and 1.9 fold to conventional treatment doses, respectively). (BM: bone marrow, HIF: hypoxia-inducible factor, SCA: stem cell antigen, VE-cadherin, vascular endothelial-cadherin, VEGFR: vascular endothelial growth factor receptor, PCR: polymerase chain reaction, FACS: fluorescence-activated cell sorting) Data = mean ± SEM (N: dots on each graph). **p* < 0.05, ***p* < 0.01, and ****p* < 0.001 between lined groups.

stabilization of HIF-1 α with consequent vasculogenic reprogramming of splenic CD11b⁺ cells.^[18] Because CoCl₂ stabilizes HIF- α expression as a hypoxic-mimetic agent,^[23] liposomes can deliver CoCl₂ into splenic CD11b⁺ cells, thereby inducing vasculogenic reprogramming upon hypoxic priming as a method of nano-hypoxia.

The hypoxia-mimetic function of CoCl₂ was examined upon priming splenic CD11b⁺ cells for 72 h in *in vitro* culture (Figure 3b). Splenic CD11b⁺ cells were isolated from mouse spleens and cultured under either no treatment or three hypoxic conditions. Compared with those in the no treat group (72 h) (Figure S5b, Supporting Information), the analysis of 50 single cells in each group exhibits that the area and aspect ratio of cells decreases significantly to the similar levels among the hypoxic chamber (72 h) and CoCl₂ treatment (72 h) without or after transferring from the no treat condition (72 h). These results indicate that the hypoxic effects of CoCl₂ treatment were similar to those of hypoxic chamber incubation in terms of inducing differentiation of splenic CD11b⁺ cells by promoting HIF-1 α expression and stability. As a result, hypoxic chamber incubation (72 h) significantly reduced CD11b expression in splenic CD11b⁺ cells, as opposed to vasculogenic marker protein [CD34 and stem cell antigen 1 (SCA1)] expression, compared with no treat condition upon immunofluorescence staining with quantitative analysis (Figure S5c, Supporting Information). The same vasculogenic effect of the hypoxic chamber was observed in the CoCl₂ treatment (72 h), with increased protein expression of HIF-1 α , CD34, and SCA1, compared to the no treat condition in immunofluorescence staining analysis (Figure 3c; Figure S5d, Supporting Information). These results were further supported by the gene expression of vasculogenic markers [CD34, SCA1, vascular endothelial (VE)-cadherin, and vascular endothelial growth factor receptor (VEGFR)] in the CoCl₂ treatment group using PCR,^[10,12] compared to the no treat group (Figure 3d).

2.5. Nano-Hypoxia for Vasculogenic Reprogramming

As a programmer of nano-hypoxia (Figure S6a, Supporting Information), CoCl₂ was loaded into coating (+) liposomes, resulting in a typical circular shape (average diameter = 126 nm) within the size range of 100–150 nm in TEM. Like CoCl₂ treatment, *in vitro* treatment of CoCl₂-coating (+) for 72 h promoted the protein expression of HIF-1 α and vasculogenic markers (CD34 and SCA1) in splenic CD11b⁺ cells, compared to the no treat group in immunofluorescence staining with quantitative image analysis (Figure S6b, Supporting Information). Next, *in vivo* nano-hypoxia was induced by injecting CoCl₂ (500 ng)-coating (+) into the mouse tail vein for 72 h (Figure 3e). Cobalt levels in the spleen, as an indication of CoCl₂-coating (+) accumulation, were increased in the injection group, in comparison with those in the no injection groups (Figure S6c, Supporting Information). In addition, CoCl₂ (42 μ M)-coating (+) did not exert the hemolysis effect as the level was like that of no treat group for 24 h in contrast to the severely damaged red blood cells even at 4 h after injection of the positive control (100 mM CoCl₂) (Figure S6d, Supporting Information). Hence, nano-hypoxia was safe during blood circulation and splenic accumulation due to the low dose (42 μ M) of CoCl₂.

As the cobalt level increases in the spleen, the mouse spleen exhibited a significant reduction in the protein expression of the CD11b marker, as opposed to that of vasculogenic marker proteins (CD34, SCA1), compared to the no treat group in immunofluorescence staining (Figure 3f). The reduction of CD11b expression indicates that the successful reprogramming by nano-hypoxia can prevent the detrimental inflammatory role of CD11b in mediating leukocyte transmigration to damage tissues. Instead, tissue regeneration can be supported by the increased expression of vasculogenic marker proteins.

This effect was compared to the surgical induction of hypoxia by ligating the splenic artery for 72 h (Figure 3g). After anesthetizing the mice, the splenic artery was identified by abdominal incision and ligated, followed by the observation of a change in spleen color to darker tones as an indication of hypoxic induction (Figure S6e, Supporting Information). Consistent with observations in the nano-hypoxia group (Figure 3h), surgical induction of splenic hypoxia significantly reduced the protein expression of myeloid markers (CD11b and CD45) as opposed to that of vasculogenic markers (CD34 and VE-cadherin), compared to the no treat group in FACS. Nano-hypoxia was more effective than surgical induction in reducing the number of CD11b⁺ cells. Compared with BM cells after extraction from the femur (i.e., conventional approach), nano-hypoxia was superior in promoting the protein expression of vasculogenic markers (CD34, VE-cadherin, or c-Kit) in splenic cells (Figure 3i). These results were further supported by comparison with the conventional treatment doses (500 000 cells) of vasculogenic cells^[9,10] (Figure 3j) because the number of CD34⁺ cells was up to 11.9 times higher in splenic nano-hypoxia compared to the BM cells (22.7 and 1.9 folds to conventional treatment doses, respectively).

2.6. Inflammation-Responsive Homing with Vasculogenic Potential

Splenic CD11b⁺ cells move to sites where inflammation occurs (“inflammation-responsive homing”). Therefore, the effect of post-vasculogenic reprogramming on homing ability was examined using *ex vivo* culture of normal and inflamed vascular tissue from an ischemic hindlimb model in a 3D hydrogel chip with microchannel, maintaining of tissue viability during 24 h of experiment (Figure S7a, Supporting Information). After vasculogenic reprogramming with CoCl₂ treatment, splenic CD11b⁺ cells (red, DiD) were injected into the site between the two tissues (green, DiO) in the hydrogel chip and cultured under medium perfusion for 24 h (Figure 4a; Figure S7b, Supporting Information). Significantly more vasculogenic cells migrated to the inflamed tissues than to the normal tissues, validating their inflammation-responsive homing ability.

Next, *in vivo* homing ability was validated using a mouse model of hindlimb ischemia (Figure 4b). CoCl₂-coating (+) (fluorescence or 19F-tagged) were injected into the tail vein (d 0), followed by femoral ligation through operation (d 3), and the homing ability was examined by tracing the amount of cobalt or liposomes. Because the hindlimb surgery was done at day 3 after tail vein injection of liposome, coating (+) was used to improve the selectivity of spleen targeting so that the sufficient

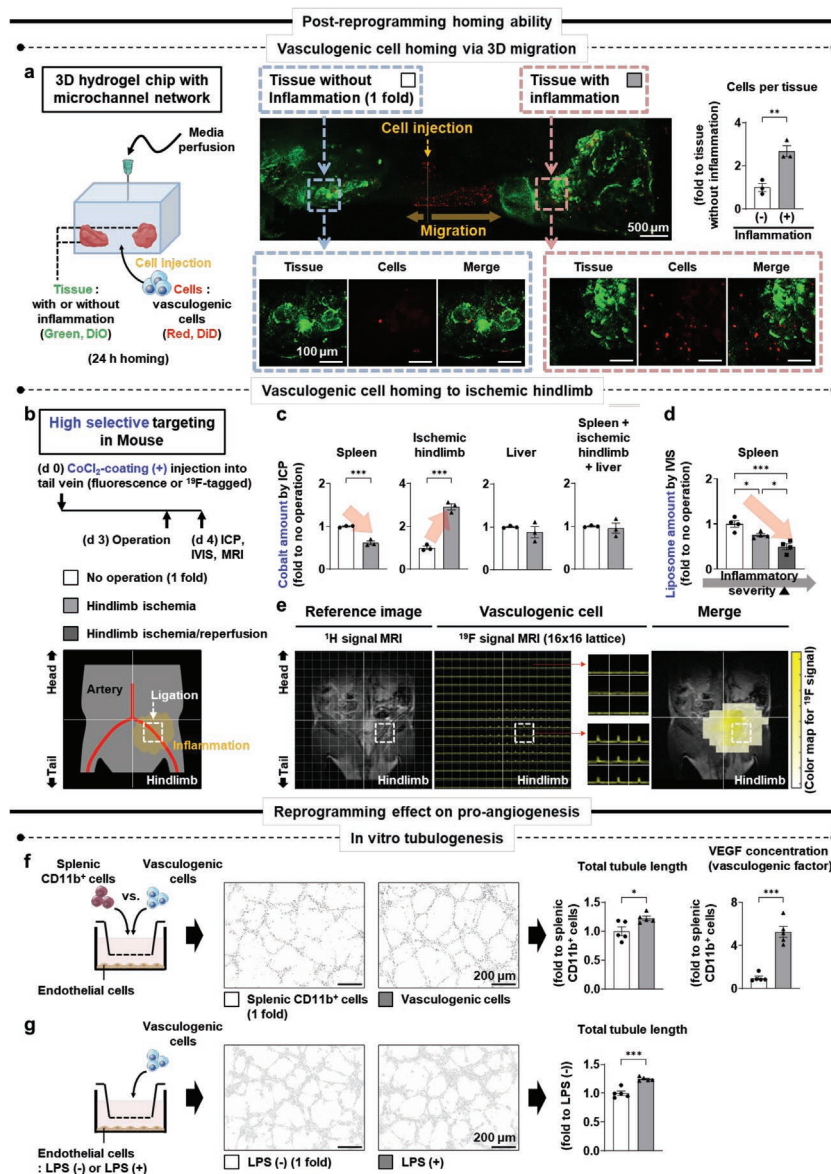


Figure 4. Inflammation-responsive homing of splenic CD11b^+ cells after vasculogenic reprogramming by nano-hypoxia. Splenic CD11b^+ cells move to sites where inflammation occurs ("inflammation-responsive homing"). Therefore, a) the effect of post-vasculogenic reprogramming on homing ability was examined using ex vivo culture of normal and inflamed vascular tissues (green, DiO) from an ischemic hindlimb model on a 3D hydrogel chip with microchannel networks. After vasculogenic reprogramming with CoCl_2 treatment, splenic CD11b^+ cells (red, DiD) were injected into the site between the two tissues on the hydrogel chip and cultured under medium perfusion for 24 h. Significantly more vasculogenic cells migrated to the inflamed tissue than to the normal tissue, validating their inflammation-responsive homing ability ($N = 3$). b) Next, in vivo homing ability was validated using a mouse model of hindlimb ischemia. CoCl_2 -coating (+) (fluorescence or ^{19}F -tagged) were injected into the tail vein (d 0), followed by femoral ligation through operation (d 3), and the homing ability was examined by tracing the amount of cobalt or liposomes. Because the hindlimb surgery was done at day 3 after tail vein injection of liposome, coating (+) was used to improve the selectivity of spleen targeting so that the sufficient liposomal dose could be delivered into the spleen beforehand to induce in situ reprogramming of CD11b^+ cells. c) The amount of accumulated cobalt in the spleen upon CoCl_2 -coating (+) injection decreased after the operation compared with that before the operation in ICP analysis ($N = 3$). The amount of cobalt in the liver and the combined amount of cobalt in the three organs (spleen, ischemic hindlimb, and liver) remained unaltered. These results indicate the inflammation-responsive homing of CD11b^+ cells occur after vasculogenic reprogramming, while maintaining the total amount of CoCl_2 -coating (+) through inter-organ circulation. d) This inflammation-responsive homing was further evidenced as the amount of splenic liposomes significantly decreased upon temporary femoral ligation (1 h) and further by reperfusion to induce paradoxical severe damage in IVIS analysis ($N = 4$). e) When ^{19}F -tagged CoCl_2 -coating (+) was traced using MRI for double confirmation, vasculogenic cells were localized geometrically around the ligation site of the femoral artery in the ischemic hindlimb (color map range: 0–800 arbitrary units). As vasculogenic cells are generated by nano-hypoxic reprogramming of splenic CD11b^+ cells, f) endothelial tubulogenesis was examined by co-culturing HUVECs in the lower chamber of a transwell (pore size = $0.4 \mu\text{m}$) with vasculogenic versus splenic CD11b^+ cells in the upper chamber for 4 h ($N = 5$). As a result, the tubule length and VEGF production increased significantly with the co-culture of vasculogenic cells, compared to those with splenic CD11b^+ cells. g) Furthermore, LPS-induced inflammation extended the total tube length of HUVECs co-cultured with vasculogenic cells in the transwell setting, compared to non-LPS treatment ($N = 5$). (ICP: inductively coupled plasma, IVIS: in vivo imaging system, MRI: magnetic resonance imaging, HUVECs: human umbilical vein endothelial cells, VEGF: vascular endothelial growth factor, LPS: lipopolysaccharide) Data = mean \pm SEM (N : dots on each graph). * $p < 0.05$, ** $p < 0.01$, and *** $p < 0.001$ between lined groups.

liposomal dose could be delivered into the spleen beforehand to induce in situ reprogramming of CD11b⁺ cells. The amount of accumulated cobalt in the spleen upon CoCl₂-coating (+) injection decreased after the operation compared with that before the operation in inductively coupled plasma (ICP) analysis (Figure 4c). The amount of cobalt in the liver and the combined amount of cobalt in the three organs (spleen, ischemic hindlimb, and liver) remained unaltered. These results indicate the inflammation-responsive homing of CD11b⁺ cells occur after vasculogenic reprogramming, while maintaining the total amount of CoCl₂-coating (+) through inter-organ circulation. This inflammation-responsive homing was further evidenced by IVIS (Figure 4d; Figure S7c, Supporting Information). The radiant intensity (range: 5–50 × 10⁷) increased in the spleen without operation as an indication of CoCl₂-coating (+) accumulation. However, the intensity in the spleen was attenuated upon the induction of hindlimb ischemia and further by reperfusion at the site of temporal femoral ligation (1 h) as the severity of inflammation increased. This result indicates the inflammation degree-dependent exit of CoCl₂-coating (+) from the spleen.

To track geometrical localization in the mouse body using MRI, perfluorohexanol was loaded into CoCl₂-coating (+), which was confirmed by a ¹⁹F chemical shift in the nuclear magnetic resonance (NMR; Figure S7d, Supporting Information). When ¹⁹F-tagged CoCl₂-coating (+) were traced in the mouse model of hindlimb ischemia using MRI for double confirmation (Figure 4e), vasculogenic cells were localized geometrically around the ligation site of the femoral artery in the ischemic hindlimb (color map range: 0–800 arbitrary units). As vasculogenic cells were generated by nano-hypoxic reprogramming of splenic CD11b⁺ cells, endothelial tubulogenesis was examined by co-culturing human umbilical vein endothelial cells (HUVECs) in the lower chamber of a transwell (pore size = 0.4 μm), with vasculogenic versus splenic CD11b⁺ cells in the upper chamber for 4 h (Figure 4f). As a result, the tubule length and vascular endothelial growth factor (VEGF) production increased significantly with the co-culture of vasculogenic cells, compared to those with splenic CD11b⁺ cells. Furthermore, LPS-induced inflammation extended the total tube length of HUVECs co-cultured with vasculogenic cells in the transwell setting compared with non-LPS treatment (Figure 4g).

2.7. Therapeutic Potential of Nano-Hypoxia

The feasibility of vasculogenic therapy was examined by applying nano-hypoxia to two damage models of mice via the injection of CoCl₂-coating (+) into the tail vein (d 0). Because both damages were given at day 3 after tail vein injection of liposome, coating (+) was used to improve the selectivity of spleen targeting so that the sufficient liposomal dose could be delivered into the spleen beforehand to induce in situ reprogramming of CD11b⁺ cells. First, for vascular therapy (Figure 5a), hindlimb ischemia was induced by femoral artery ligation (d 3) with or without BM cell injection for comparison, followed by sacrifice (d 17). Laser Doppler imaging was performed on days 3, 10, and 17, and the toxicity of CoCl₂ was examined on days 3 and 17. The endpoint evaluation was conducted using MRI and

histopathology on day 17. Second, for liver therapy (Figure 5b), 70% of the liver was resected (hepatectomy, d 3) with or without splenectomy (nano-hypoxia + splenectomy) for comparison, followed by sacrifice (d 5 and 7). Computed tomography (CT) was performed on days 3 and 7, and the expression of liver functional markers was examined on day 7 with endpoint evaluation by histopathology on days 5 and 7.

When BM cells were compared using the conventional approach, in addition to the no treat group (d 17), nano-hypoxia substantially increased cell invasion into the ischemic hindlimb, as evidenced by the number of nuclei in H&E staining (Figure S8a, Supporting Information). In the ischemic hindlimbs, nano-hypoxia promoted the protein (Figure 5c; Figure S8b, Supporting Information) and gene expression (Figure 5d) of angiogenic markers [CD31 and von Willebrand factor (vWF)], compared with no treat and BM cell groups, as evidenced by immunofluorescence staining and PCR, respectively. Consequently, flow patency increased from the no treat group to the BM cell group and further to the nano-hypoxia group, indicating efficient rescue of limb damage by nano-hypoxia over 17 days, as evidenced by laser Doppler imaging with quantitative analysis (Figure 5e; Figure S8c, Supporting Information). These results were confirmed by MRI (3D and 2D) on day 17 (Figure 5e).

Most nanoparticles are cleared through the liver; thus, cobalt toxicity in the liver was examined after systemic circulation, although the cobalt level was ≈25 μg kg⁻¹, which is far below the toxic range (500–4000 μg kg⁻¹).^[24–26] When CoCl₂-coating (+) were injected into the mouse tail vein, cobalt level in the liver intensified, indicating CoCl₂-coating (+) accumulation on day 3 (Figure S8d, Supporting Information). However, CoCl₂-coating (+) injection did not increase the blood secretion of liver failure markers (aspartate aminotransferase, alanine aminotransferase, alkaline phosphatase, and bilirubin) early on day 3 (Figure S8e, Supporting Information) and on day 17 at the end of the experiment (Figure S8f, Supporting Information), compared to the no treat group.

Blood vessel formation is a key requirement for liver regeneration, owing to its vessel-rich tissue structure. Hence, 70% of the mouse liver was resected, as confirmed by the volume reduction at day 3 in contour images (Figure S9a, Supporting Information). In the resected liver, nano-hypoxia increased the protein expression of angiogenic markers (CD31, vWF, and VEGF) over 7 days, compared to the no treat group, as determined by immunofluorescence staining (Figure 5f; Figure S9b,c, Supporting Information). However, splenectomy diminished this therapeutic effect to the level of the no treat group, indicating that the spleen is the major reservoir of vasculogenic cells.

Nano-hypoxia generated more mitotic features in hepatic cells on day 5, as examined by H&E staining (Figure S9d, Supporting Information), and the protein expression of the proliferation marker (Ki-67) was significantly increased in hepatic cells on day 5 (Figure 5g; Figure S9e, Supporting Information) on immunofluorescence staining. Upon sacrifice on day 7, the nano-hypoxia group exhibited a significantly larger liver size on CT (Figure 5h), with heavier liver weight (per body weight) (Figure 5i) and lower expression of the liver failure marker (bilirubin) in the blood (Figure 5j), compared to the no treat group.

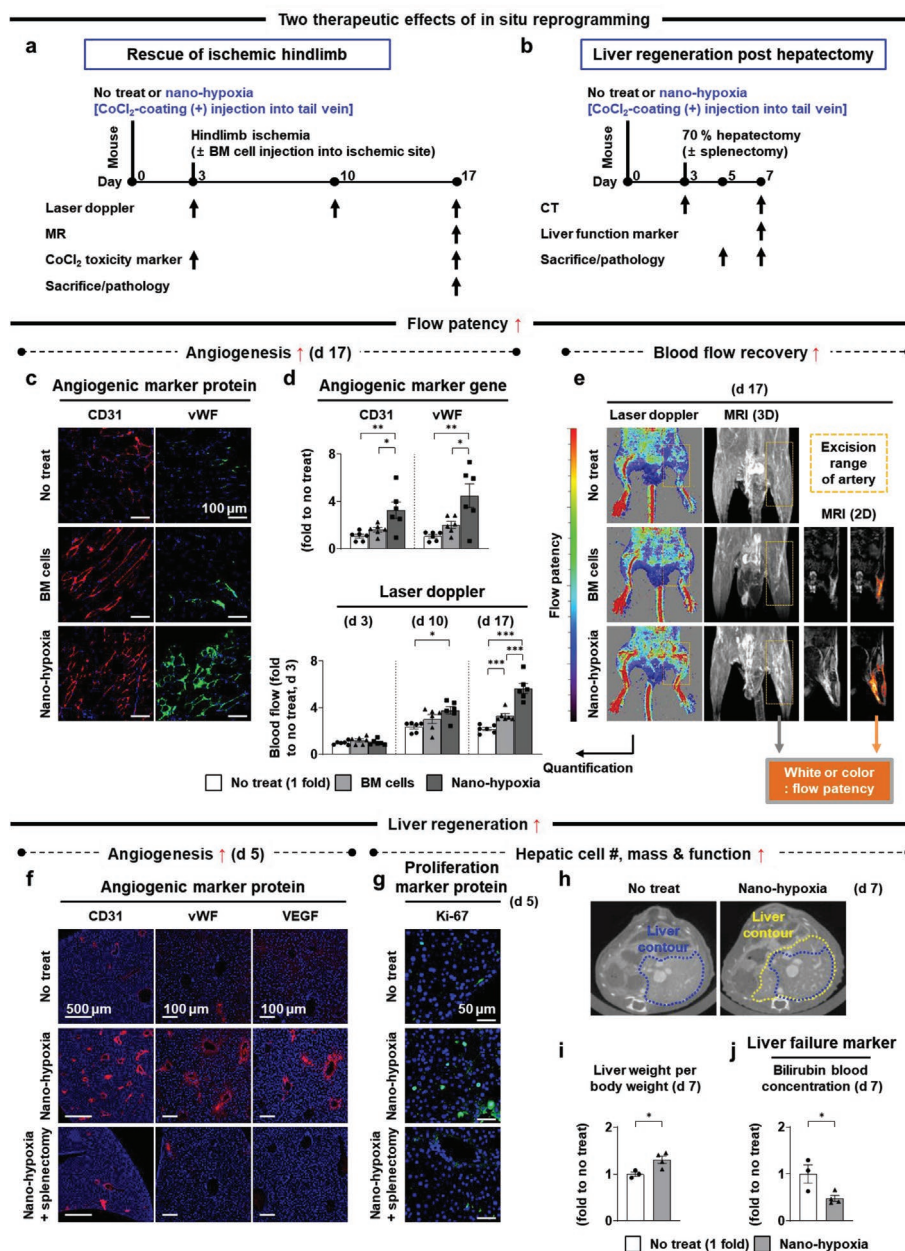


Figure 5. Therapeutic effects of nano-hypoxia on ischemic hindlimb and liver damage by in situ vasculogenic reprogramming. The feasibility of vasculogenic therapy was examined by applying nano-hypoxia to two damage models of mice via the injection of CoCl₂-coating (+) into the tail vein (d 0). Because both damages were given at day 3 after tail vein injection of liposome, coating (+) was used to improve the selectivity of spleen targeting so that the sufficient liposomal dose could be delivered into the spleen beforehand to induce in situ reprogramming of CD11b⁺ cells. a) First, for vascular therapy (N = 6), hindlimb ischemia was induced by femoral artery ligation (d 3) with or without BM cell injection for comparison, followed by sacrifice (d 17). Laser Doppler imaging was performed on days 3, 10, and 17, and the toxicity of CoCl₂ was examined on days 3 and 17. The endpoint evaluation was conducted using MRI and histopathology on day 17. b) Second, for liver therapy (N = 3–4), 70% of the liver was resected (hepatectomy, d 3) with or without splenectomy (nano-hypoxia + splenectomy) for comparison, followed by sacrifice (d 5 and 7). CT was performed on days 3 and 7, and the expression of liver functional markers was examined on day 7 with endpoint evaluation using histopathology on days 5 and 7. In ischemic hindlimbs, nano-hypoxia promoted the c) protein and d) gene expression of angiogenic markers (CD31 and vWF), compared with the no treat and BM cell groups in immunofluorescence staining and PCR, respectively. e) This vasculogenic potential of nano-hypoxia significantly promoted blood flow recovery as evidenced by using laser Doppler imaging and MRI (3D and 2D) with quantitative analysis on day 17, compared to the no treat and BM cell groups. In the resected liver, f) nano-hypoxia increased the protein expression of angiogenic markers (CD31, vWF, and VEGF) compared to the no treat group on day 5 in immunofluorescence staining. However, splenectomy diminished this therapeutic effect to the level of the no treat group, indicating that the spleen is the major reservoir of vasculogenic cells. g) These results are aligned with hepatocyte proliferation examined based on the protein expression of the proliferation marker (Ki-67) using immunofluorescence staining. Upon sacrifice on day 7, the nano-hypoxia group exhibited h) significantly larger liver size on CT, i) with heavier liver weight (per body weight), and j) lower expression of the liver failure marker (bilirubin) in the blood, compared to the no treat group. (BM: bone marrow, MRI: magnetic resonance imaging, CT: computed tomography, vWF: von Willebrand factor, PCR: polymerase chain reaction, VEGF: vascular endothelial growth factor). Data = mean ± SEM (N: dots on each graph). **p* < 0.05, ***p* < 0.01, and ****p* < 0.001 between lined groups.

These results indicate the efficient therapeutic effect of nano-hypoxia in rescuing the inflamed hindlimb and regenerating the severely damaged liver.

3. Discussion

The present study aimed to provide a turning point strategy by addressing the unmet needs in the current field of nano-delivery based on the following cause-and-effect thread of ideas. First, the spleen was approached as a reservoir^[1] of second carriers by reverting the clearance issue in the inevitable splenic filtering of nanoparticles to the advantageous concept of targeting the reservoir spontaneously. To deliver the first carrier (i.e., liposome) of cargo to this reservoir of the second carrier (i.e., splenic CD11b⁺ cell), a single injection into the vein led to accumulation of first carriers through in-body circulation, thereby avoiding repeated or continuous injections. This spontaneous splenic targeting was independent of nanoparticle type, as confirmed using nanovesicles from TMSCs. Hence, liposomes were used in this approach, considering their validated utilities for most clinical applications. When liposomes and nanovesicles approached splenic targeting, the negative impression of non-PEGylation in the form of coating (–) was reversed to enable rapid targeting to the spleen up to 12 h post-injection. Skin inflammation was induced before liposomal injection to establish a model to require immediate rescue by fast targeting. The fast targeting of coating (–) was accelerated to increase the liposomal distribution into the site of LPS-gel implantation in the inflammation degree-dependent manner, thereby validating the utility of fast targeting. In contrast, splenotropic targeting of the coating (+) liposome^[5,6] was used to improve the selectivity of splenic targeting for a prolonged period. The hindlimb ischemia and hepatectomy were carried out on day 3 after tail vein injection of liposome, thereby validating the utility of coating (+) as a means to improve the selectivity of spleen targeting. The results indicate that a sufficient liposomal dose was delivered into the spleen to induce in situ reprogramming of CD11b⁺ cells. In this way, the speed and selectivity of splenic targeting by liposomes can be controlled depending on the need for either burst or sustained effects in case-specific therapies^[27] toward broad applications.^[4]

Second, splenic targeting by liposomes enabled the strategy of carrier change to improve the duration and accuracy of cargo delivery using splenic CD11b⁺ cells, thereby addressing the current issue of rapid clearance of nanoparticles. This approach is a mimetic model of an aircraft carrier, i.e., sending an aircraft upon sensing the target, thereby improving the duration and accuracy of bomb attacks. Furthermore, the use of CD11b⁺ cells (i.e., aircraft) as the second carrier from the spleen (i.e., aircraft carrier) enables inflammation-responsive delivery of the cargo (e.g., theranostic agents, such as bombs) carried by the first carrier (i.e., liposome). As CD11b⁺ cells naturally move to the precise sites of inflammation on time, this approach further improves the targeting accuracy with the advanced function of stimulus-responsive targeting.

Third, nano-hypoxia was established as a therapeutic means by combining the aforementioned strategies based on the following rationales including i) a causative role of hypoxia in cell

differentiation, including CD11b⁺ cells to vascular or vasculogenic lineages,^[17–20] ii) spleen as a reservoir of CD11b⁺ cells,^[1] and iii) rich therapeutic indications of CD11b⁺ cells in the treatment of vascular diseases.^[9–12] Clinical trials have demonstrated only a marginal effect of CD11b⁺ cells,^[13,14] possibly due to the limited number of harvested cells,^[15,16] with therapeutic efficacy being downgraded by cell senescence during lengthy propagation. The encapsulation efficiency of CoCl₂ in coating (+) liposomes was ≈42%, and the loading amount of CoCl₂ should be maximized but biocompatible during blood circulation and splenic accumulation. Because the 100 mM of CoCl₂ appeared to be non-biocompatible as evidenced by the hemolysis effect (Figure S6e, Supporting Information), 42 μM of CoCl₂ (500 ng) was used as the delivery dose by considering the 42% encapsulation efficiency and the consequent biocompatibility with red blood cells and CD11b⁺ cells. Indeed, this dose reprogrammed splenic CD11b⁺ cells into vasculogenic cells more than 10-fold effectively compared to the conventional strategy using 500 000 vasculogenic cells (Figure 3j), and the therapeutic effects of reprogramming were validated in maintaining the vasculogenic homing to inflamed sites and rescuing the two damage models (Figures 4 and 5).

Finally, the inflammation-responsive homing ability of splenic CD11b⁺ cells remained unaltered even after vasculogenic reprogramming. This advantage addresses another unmet need of clinical studies because invasive angiography has been used to deliver cells to ischemic sites,^[13,14] with a risk of hemorrhage and thrombosis. Microchannel hydrogel chips enabled the 3D culture of normal versus inflamed tissues *ex vivo*, so that the homing ability could be directly observed by excluding other factors in the systemic circulation *in vivo*. The zoomed, close, and real-time validation of inflammation-responsive homing ability can serve as a foundation to approach the vasculogenic therapy, as examined in models of ischemic hindlimbs and extensive liver damage. A small dose of CoCl₂ did not cause liver toxicity for up to 17 days post-injection and exerted highly effective and efficient therapeutic effects, representing another selling point of nano-hypoxia. In addition to this evidence towards successful translation, the effects of nano-hypoxia were validated in a step-by-step manner using fundamental and clinical tools, including IVIS, TEM, intravital multi-photon microscopy, and 2D/3D MRI with multiple imaging agents (i.e., fluorescence, gold nanoparticles, and ¹⁹F).

Despite the series of advantages associated with validation, large animal models of vascular therapy and regeneration are warranted in future studies. Long-term effects of nano-hypoxia remain to be elucidated, as mouse models in the present study were established by considering the typical duration of angiogenesis and hepatocyte growth. In particular, the stabilization of HIF-1α by nano-hypoxia may lead to unexpected outcomes in several organs, including adverse cardiac remodeling, pulmonary hypertension, liver fibrosis, and epithelial-mesenchymal transition in kidney.^[28,29] Hence, these possible side effects should be examined thoroughly in a large animal model to improve the translational potential. As a hypoxic-mimetic agent, CoCl₂ was selected to improve the expression and stabilization of HIF-1α because its atomic number is similar to that of Fe²⁺. However, other candidates, including genetic alteration and small molecules, should be examined in future studies.

Although hypoxia chamber, surgical induction of splenic hypoxia, and two mouse models of ischemic damage were used as controls to compare with nano-hypoxia, multi-spot incidences of hypoxic damage warrant further investigation, as disease occurrence is spatiotemporally sporadic in the body. One idea for the next study could be to increase the loading concentration of CoCl_2 over the current hemato-compatibility level (500 ng) so that blood cells can be damaged upon uptake of CoCl_2 -coating (+), which then undergoes spontaneously splenic filtering with CoCl_2 by CD11b^+ cells, thereby increasing the period and power loading of carrier change. In addition, the spontaneous clearance of circulating liposomes through the spleen with CD11b^+ cells were strategized to approach the concept of carrier change as the spleen serves as a reservoir of CD11b^+ cells (i.e., the second carrier) that moved to the inflamed sites upon the damages. Nonetheless, the roles of other clearance organs (liver, lung, etc.) in changing the carrier from liposome to CD11b^+ cells in a large capacity will be investigated further.

4. Experimental Section

Suppliers: Suppliers of antibodies, staining reagents, and single items were denoted with the corresponding items.

Sigma-Aldrich (St. Louis, MO, USA) supplied 1,2-dipalmitoyl-sn-glycero-3-phosphocholine (DPPC; 850355P), cholesterol (C8667), 1,2-distearoyl-sn-glycero-3-phosphoethanolamine (DSPE; 850715P), 1,2-distearoyl-sn-glycero-3-phosphoethanolamine-N-[methoxy(polyethylene glycol)-2000] (DSPE-PEG; 880120P), ethanol (E7023), CoCl_2 (C8661), gold nanoparticle solution (752568), 1H,2H,2H,2H-perfluorohexanol (532770), Avanti mini-extruder (610000), filter support (610014), ferric chloride hexahydrate (F2877), ammonium thiocyanate (221988), methoxy-polyethylene glycol (mPEG; 202495), ϵ -caprolactone (704067), tin(II) 2-ethylhexanoate (S3522), dichloromethane (270997), diethyl ether (179272), lipopolysaccharide (LPS; L4391), albumin (A9771), poly-L-lysine-coated 24 well plate (P8920), DNase I (D4263), CoCl_2 solution (for cell culture; 15862), Poly(N-isopropylacrylamide) (PNIPAM; 535311), gelatin (G1890), Triton X-100 (93443), and RIPA buffer (R0278).

Merck Millipore (Burlington, MA, USA) supplied methanol (106009) and bovine serum albumin (BSA; 82-100-6). Welgene (Gyeongsan, Republic of Korea) supplied phosphate-buffered saline (PBS; LB004) and Dulbecco's PBS (DPBS; LB001). Korea Vaccine Co., Ltd. (Seoul, Republic of Korea) supplied 20- and 26-gauge needles. Steritech (Auburn, WA, USA) supplied polycarbonate membrane filters (100 nm: PCT019030 and 5 μm : PCT509030).

Thermo Fisher (Waltham, MA, USA) supplied DiD (V22887), automated cell counter (Countess II), Dulbecco's modified Eagle's medium (DMEM; for RAW 264.7 cells: 11995-065; for tonsil-derived mesenchymal stem cells (TMSCs): 11885-084), fetal bovine serum (FBS; 16000-044), penicillin-streptomycin (15140-122), collagenase type I (17100-017), 0.25% trypsin-EDTA (25200-072), BCA protein assay kit (23227), Neon electroporation system (MPK5000), RPMI 1640 medium (11875-093), hypoxia incubator (4131), DiO (V22886), Live & Dead assay kit (L3224), and Trizol (15596018).

Perkin Elmer (Waltham, MA, USA) supplied UV-vis spectrophotometry (Lambda 25), ICP (Nexion 2000), IVIS (124262), and CT (Quantum GX2) platforms. Bruker (Billerica, MA, USA) supplied NMR (Avance III HD 400) and MRI (9.4 T BioSpec) platforms. Orient Bio (Gyeonggi-do, Republic of Korea) supplied the BALB/c and C57BL/6 mice. Carl-Zeiss (Oberkochen, Germany) supplied confocal microscopes (intravital multiphoton microscopy: LSM 7MP; confocal microscopy: LSM 980) and ZEN software (V3.0). Corning (Steuben County, NY, USA) supplied centrifuge tubes (PCR-05-C and MCT-175-C) and Matrigel (354234). Ailee (Busan, Republic of Korea) supplied 4-0

black silk (SK434) and 6-0 black silk (SK517). GE Healthcare (Chicago, IL, USA) supplied MRI and CT contrast media (Clariscan and Iodixanol, respectively).

SPL (Seoul, Republic of Korea) supplied a 70 μm strainer (93070) and transwell inserts (35024). Cytiva (Freiburg, Germany) supplied Ficoll-Paque (17144002) and a biomolecular imager (ImageQuant 800). Lonza (Basel, Switzerland) supplied HUVECs and the EGM-2 Bullet Kit (CC-3162). Biosesang (Seongnam, Republic of Korea) supplied 10% neutral-buffered formalin (F2013) and pure water (WR2006). Bio-Rad Laboratories (Hercules, CA, USA) supplied the SDS-PAGE gel (4561094), protein ladder (1610394), skim milk (1706404), and enhanced chemiluminescence substrate kit (1705060). Invitrogen (Waltham, MA, USA) supplied nitrocellulose membranes (IB23001), a gel transfer device (iBlot2), and EDTA (15575-038). Applied Biosystems (Waltham, MA, USA) supplied a real-time PCR system (StepOne V2.3) and SYBR Green PCR mix (4367659). BD Bioscience (Mississauga, Canada) supplied FACS (LSRII) platform and FlowJo software (V10).

Liposome Preparation: Liposomes were prepared via either lipid film hydration or rapid injection for liposomes without and with cargo, respectively by using the lipid mixture with DPPC, cholesterol, and DSPE (– coating) or DSPE-PEG (+ coating).

Lipid film hydration was conducted by dissolving the 55:40:5 molar ratio of DPPC, cholesterol, and DSPE (– coating) or DSPE-PEG (+ coating) in a 2:1 (v/v, 10 mL) solution of chloroform (6955, Duksan, Ansan, Republic of Korea) and methanol in a glass round-bottom flask connected to a rotary evaporator (WEV-1001V, Daihan Scientific, Wonju, Republic of Korea) with immersion in a water bath. A lipid film was produced using a vacuum pump (under 500 mbar) through evaporation of solvents for overnight; In this overnight step, for slow evaporation to make a thin and even lipid film, vent hole was opened for first 60 min. Also, rotation speed was 90 rpm for first 60 min and increased to 180 rpm, and the water bath was set to 45 °C for first 90 min and turned off. Next day, the lipid film was hydrated by adding 10 mL of PBS under 30 min rotation, and the flask was then detached from the rotary evaporator and sonicated (UCP-10, Jeio Tech, Daejeon, Republic of Korea) at 45 °C for 30 min.

Rapid injection was performed to load cargos into liposomes by first dissolving DPPC, cholesterol and DSPE-PEG in 200 mmol L^{−1} of lipid mixture in ethanol at 72 °C at the molar ratio of 55:40:5. The cargo-containing solution was prepared by adding either CoCl_2 (1 M) or a gold nanoparticle (diameter = 5 nm) solution. The lipid mixture was then rapidly injected using a 20-gauge needle with a syringe (Restek, Bellefonte, PA, USA) into the same volume of cargo-containing solution under vigorous stirring (500 rpm) at 72 °C for 5 min. Next, quadruple volume of the same type of cargo solution was reacted under stirring for 15 min at room temperature. CoCl_2 -coating (+) were tagged with ¹⁹F in a 19:1 (v/v) solution of ethanol and 1H,2H,2H,2H-perfluorohexanol-1-ol, or liposomes were labeled with DiD following the manufacturer's instructions.

Liposome size was controlled by extruding 12 times through a polycarbonate membrane filter with a pore diameter of 100 nm using an Avanti mini-extruder and filter support. In case of cargo-loading, unloaded cargos were removed by overnight tube dialysis (molecular weight cutoff = 12–14 kDa; 132706, Repligen, Waltham, MA, USA). Liposomes were collected by centrifugation at 30000 × g for 1 h at 4 °C and resuspended in PBS and normal saline (JW Pharmaceutical, Seoul, Republic of Korea) for in vitro and in vivo use, respectively.

Liposome Characterization: The concentration of liposomes was determined using the Stewart assay^[30] by dissolving liposomes or standard lipid samples in chloroform. Next, a ferrothiocyanate reagent was prepared by dissolving 27.03 g of ferric chloride hexahydrate and 30.4 g of ammonium thiocyanate in 1 L of deionized water. These two solutions were mixed by vortexing for 20 s and centrifuged at 300 × g for 10 min to separate the two phases. Absorbance of the lower liposome phase in chloroform was determined at 485 nm using an UV-vis spectrophotometer.

The morphology and size of the liposomes were examined by TEM (Jem2100, JEOL, Tokyo, Japan) and nanoparticle tracking analysis (NS300, Malvern Panalytical, Malvern, UK). The loading stability and amount of cargo in liposomes were examined by ICP and NMR for CoCl₂ and ¹⁹F (dissolved in D₂O), respectively.

Animal Experiments: All animal experiments were approved by the Institutional Animal Care and Use Committee of the Yonsei University College of Medicine (Permit No. 2019-0205, 2022-0050). Mice (BALB/c or C57BL/6, male, 6 weeks old) were anesthetized by either inhalation of isoflurane (Ifran, Hana Pharm, Seongnam, Republic of Korea) or intraperitoneal injection of zoletil (50 mg kg⁻¹; Virbac, Seoul, Republic of Korea) and xylazine (10 mg kg⁻¹; Bayer, Leverkusen, Germany), followed by tail vein injection of liposomes (200 µL of 1 mM liposome, or otherwise specified). Fluorescence-tagged liposomes were injected into the mice after feeding a diet without autofluorescence (D10001, Central Lab. Animal Inc., Seoul, Republic of Korea) for a week. The mice were sacrificed using CO₂ at the end of each experiment.

Liposomal Targeting to the Spleen: Liposomal targeting to splenic CD11b⁺ cells was examined by injecting fluorescence-tagged liposomes into the mouse tail vein, followed by IVIS analysis to determine liposomal distribution in the organs upon sacrifice.

Intravital imaging was applied to monitor the speed of liposomal targeting by closely exposing the spleen to the lens of a multiphoton microscope after anesthetizing the mice with an abdominal incision. First, reference imaging of CD11b⁺ cells was performed by injecting 100 µL of anti-CD11b-FITC (1:200; MA1-10081, Thermo Fisher) into the bolus. An intravenous injection line (BB31695-PE/I, Scientific Commodities, Lake Havasu City, AZ, USA) was connected to the tail vein. Then, upon starting image acquisition in the spleen, liposomes (1 mM) were continuously injected into the tail vein at 200 µL min⁻¹ through the line with a syringe pump (Pump 11 Pico Plus Elite, Harvard Apparatus, Holliston, MA, USA). Signal intensity was recorded every second, followed by quantitative analysis using ZEN software.

After harvesting, the spleen was subjected to frozen section and immunofluorescence staining with DAPI (H1200, Vectashield, Darmstadt, Germany) and anti-CD11b-FITC (1:200) with secondary anti-mouse Alexa Fluor 594 (1:500; 115-585-003, Jackson Lab, Bar Harbor, ME, USA), as described below. In the case of liposomal loading with gold nanoparticles, the spleen was imaged using TEM.

Splenic monocytes were isolated using a monocyte isolation kit (19861A, Stemcell Technologies, Vancouver, Canada) and stained with DAPI and wheat germ agglutinin (1:200; 29022, Biotium, Fremont, CA, USA). CD11b⁺ cells were separated from other splenic cells using the CD11b selection kit (480110, BioLegend, San Diego, CA, USA).

Inflamed Skin Model: As a depot of pro-inflammatory agent (LPS) under implantation, and mPEG-poly(caprolactone) (mPEG-PCL) hydrogel was synthesized by reacting to 10 mmol of mPEG and 100 mmol of ε-caprolactone using 0.1 g of tin(II) 2-ethylhexanoate as a catalyst. The mixture was heated to 140 °C for 90 min under nitrogen atmosphere, followed by cooling to room temperature. The mixture was then dissolved in 15 mL of dichloromethane and precipitated using 800 mL of diethyl ether at 4 °C, followed by vacuum drying for 24 h. The precipitate was dissolved in PBS (0.2% w/w), heated to 80 °C for 10 min, and cooled down.

After anesthetizing the mice and shaving the skin, the mPEG-PCL hydrogel (200 µL per shot) with LPS was subcutaneously injected using a 26-gauge needle to establish a mouse model of inflamed skin. The next day, fluorescence-tagged liposomes were injected and maintained until imaging, staining, and molecular examination of the harvested organs. Immunofluorescence staining was performed on paraffin sections using DAPI and anti-CD11b-FITC (1:200), and FACS analysis was performed by staining the cells with anti-CD11b-FITC (1:500), as described below.

In Situ Reprogramming of Splenic CD11b⁺ Cells: In situ reprogramming of splenic CD11b⁺ cells by nano-hypoxia were examined by injecting CoCl₂ (500 ng)-coating (+) BM cells were extracted from mouse femurs as the representative conventional approach for comparison. After sacrificing the mice and dissecting the surrounding muscles, ligaments, and tendons, the lower end of the femur was excised to expose the marrow

cavity, and the femur was harvested into a centrifuge tube (0.5 mL) by drilling a hole at the bottom using a 20-gauge needle. This tube was inserted into a larger (1.7 mL) centrifuge tube and then centrifuged at 10000 × g for 15 s to drain the marrow through the bottom hole of the small tube into the large tube. As a surgical model for comparison, splenic hypoxia was induced through an operation to expose the spleen under microscopic monitoring after anesthetizing the mice with abdominal incision. The splenic artery was then identified and ligated two times using 9-0 ethilon (2829G, Ethicon, Raritan, NJ, USA), followed by the closure of the abdomen using 4-0 black silk.

After sacrificing the mice, the spleens were harvested and subjected to immunofluorescence staining on frozen sections using DAPI, anti-CD11b (1:200; ab8878, Abcam, Waltham, MA, USA), anti-CD34 (1:200; ab81289, Abcam), and anti-SCA1 (1:200; ab51317, Abcam). Then, secondary anti-rat Alexa Fluor 594 (1:500; 712-585-150, Jackson Lab) and anti-rabbit Alexa Fluor 488 (1:500; 111-545-003, Jackson Lab) were used as described below. In addition, FACS analysis was performed after harvesting cells from the corresponding tissues (spleen and BM) and counting the number of cells using an automated cell counter. The cells were stained with anti-CD11b-FITC (3 µg mL⁻¹), anti-CD45-allophycocyanin (APC) (2.5 µg mL⁻¹; 147708, Biolegend), anti-CD34-phycoerythrin (PE)-cyanine 7 (5 µg mL⁻¹; 119326, Biolegend), anti-VE-cadherin-PE-cyanine 7 (10 µg mL⁻¹; 138016, Biolegend), and anti-c-Kit-APC-cyanine 7 (2.5 µg mL⁻¹; 135136, Biolegend) following the process described below.

Hindlimb Ischemia Model: After anesthetizing the mice with a skin incision, the upper and lower points of the femoral artery and vein were ligated using 6-0 black silk, followed by closure of the skin using 4-0 black silk. Meanwhile, hindlimb ischemia/reperfusion was induced by temporally ligating the upper point of the femoral artery and vein for only 1 h, followed by reperfusion to induce severe paradoxical damage at the ischemic site.

The homing ability of post-reprogrammed (vasculogenic) CD11b⁺ cells from the spleen to the inflamed, ischemic hindlimb was assessed by injecting CoCl₂-coating (+) without and with fluorescence or ¹⁹F tagging in the mouse tail vein 72 h before surgery. The mice were sacrificed 24 h post-surgery. ICP and IVIS analyses were used to determine cobalt amount and fluorescence intensity in the spleen, liver, and ischemic hindlimb. MRI was conducted to examine the ischemic limbs of ¹⁹F-tagged CoCl₂-coating (+)-treated mice under anesthetization by isoflurane inhalation. A ¹H/¹⁹F transceiver surface coil was used to acquire T2-weighted reference ¹H images following the fast spin-echo protocol. Then, the coil was tuned to ¹⁹F frequency for spectroscopic imaging using the following parameters: 40 × 40 mm field of view, free induction decay mode, 1000 ms repetition time, 50000 Hz spin echo, and 1800 scans with 41 averages. Spectra were acquired for the voxel size of 8 × 8, which were then processed to 16 × 16. The data were further analyzed using MATLAB (MathWorks, Natick, MA, USA).

The therapeutic effect of nano-hypoxia was examined by injecting CoCl₂-coating (+) as described above, while BM cells (10⁷ cells in 100 µL) were directly injected into the ischemic hindlimb before closing the skin. Laser Doppler imaging (Moor Instruments, Devon, UK) was used to determine the blood flow on days 0, 7, and 14 after surgery in mice anesthetized with zoletil (50 mg kg⁻¹) and xylazine (10 mg kg⁻¹). After injecting 200 µL of MRI contrast (Clariscan) into the tail vein, MRI was used to determine the blood flow on day 14 after surgery under anesthetization by isoflurane inhalation. T1-weighted images were acquired using the following parameters: 50 × 50 × 15 mm field of view, 256 × 150 × 20 matrix size, 13.820 ms repetition time, 1.818 ms echo time, 19.8 ° flip angle, signal average, and 5 min 13 s scan time. The biosafety of CoCl₂-coating (+) was determined on days 3 and 17 after injection by measuring the blood concentrations of aspartate aminotransferase, alanine aminotransferase, alkaline phosphatase, and bilirubin using an automated clinical chemistry analyzer (DRI-CHEM NX500i, Fuji Film, Tokyo, Japan). Also, after sacrificing the mice on day 14 post-surgery, tissues from the ischemic hindlimb were subjected to H&E staining and PCR. The results were confirmed by immunofluorescence staining of paraffin sections with DAPI, anti-CD31 (1:100; NB600-562, Novus,

Centennial, CO, USA), and anti-vWF (1:1000; NB600-586) and then by secondary anti-mouse Alexa Fluor 594 (1:500) and anti-rabbit Alexa Fluor 488 (1:500), as described below.

Partial Hepatectomy Model: The liver regenerative effect of nano-hypoxia was examined through 70% hepatectomy in mice after exposing and resecting the left lateral and median lobes using a bipolar vessel sealing instrument (LigaSure Technology, Medtronic, Dublin, Ireland) under anesthesia after skin shaving and incision. The spleen was removed from the day 0 group using a bipolar vessel-sealing instrument. Otherwise, the peritoneum and skin were serially closed using 4-0 black silk. The nano-hypoxia group was produced by injecting CoCl₂-coating (+) into the mouse tail vein 72 h before hepatectomy and maintained until sacrifice at either 48 or 96 h after hepatectomy as hepatocytes proliferates to a peak level for the initial 48 h^[31] so the consequent liver regeneration can be allowed later on until 96 h.

As an indication of liver regeneration, the incremental liver size was examined through CT before (control), immediately after (d 0), and 96 h after hepatectomy with the introduction of CT contrast (Iodixanol, 200 μ L). Upon sacrifice with liver harvest, the liver-to-body weight ratio was determined for each group. Recovery of liver function was determined by measuring the blood concentration of bilirubin 96 h after hepatectomy. Proangiogenic and pro-proliferative effects in each group were determined by H&E staining, as confirmed by immunofluorescence staining of paraffin sections with DAPI, anti-CD31 (1:100), anti-vWF (1:1000), anti-VEGF (1:200; ab2349, Abcam), and anti-Ki-67 (1:200; ab16667, Abcam) and then by secondary anti-mouse Alexa Fluor 594 (1:500) and anti-rabbit Alexa Fluor 488 (1:500), as described below.

In Vitro Effects of Coating (+/–) Liposome: The effect of hydrophilic coating of liposomes on the reduction of protein adsorption was determined by first incubating coating (+) versus (–) liposomes (500 μ L of 100 μ M) with albumin solution (500 μ L of 0.2% w/w in PBS) for 6 h. Then, the amount (% to total) of free-albumin was determined by measuring the particle sizes below (free-albumin) and above (liposome +/- albumin) 100 nm using dynamic light scattering (ELS-Z1000, Otsuka Electronics, Tokyo, Seoul). Moreover, an albumin-coated plate was prepared by loading albumin solution (200 μ L of 0.2% w/w in PBS) into each well of a poly-L-lysine-coated 24-well plate and incubating overnight at 37 °C, followed by washing twice with PBS. Then, coating (+) versus (–) liposomes (200 μ L of 250 μ M) were incubated in the albumin-coated plates for 6 h at 37 °C. The liposome solution was retrieved from each well, and the concentration of non-attached liposomes was determined using the Stewart assay to calculate the proportion (% to total) of plate-attached liposomes.

The effect of hydrophilic coating on liposome macrophage uptake was determined. RAW 264.7 cells (40071, Korean Cell Line Bank, Seoul, Republic of Korea) were seeded (4×10^5 cells per well) with or without inflammatory LPS treatment (5 μ g per well) into a 24-well glass bottom plate (P24-1.5P, Cellvis, Mountain View, CA, USA) in DMEM with FBS (10% w/v) and penicillin–streptomycin (1% w/v). After 24 h of incubation (5% CO₂, 37 °C), the medium was removed, and coating (+) versus (–) liposomes (500 μ L of 35 μ M) were incubated in each well for 6 h, followed by PBS washing two times for immunofluorescence staining following the process described below.

Coating (+/–) Nanovesicles: To validate that the hydrophilic coating effect was not specific to liposomes, nanovesicles were produced using human TMSCs. With the approval of the Institutional Review Board of Yonsei University College of Medicine (Permit No. 4-2019-1260), tonsil tissues were obtained with written consent from patients undergoing tonsillectomy. Tonsil tissues were washed three times with PBS, followed by scissor chopping and incubation with collagenase type I (210 U mL^{–1}) and DNase I (10 μ g mL^{–1}) for 2 h at 37 °C with stirring in DMEM with penicillin–streptomycin (1% w/v). The tissue solution was passed through a 70 μ m strainer, centrifuged at $300 \times g$ for 3 min, and washed two times using DMEM with FBS (10% w/v) and penicillin–streptomycin (1% w/v). The medium was then carefully poured into 20 mL of Ficoll–Paque reagent and centrifuged at $300 \times g$ for 20 min. Buffy coat was obtained and washed using DMEM with FBS (10% w/v) and

penicillin–streptomycin (1% w/v), and TMSCs were cultured to reach 80%–90% confluence (passage 3–6) in an incubator (5% CO₂, 37 °C).

Nanovesicles were produced by detaching TMSCs using trypsin-EDTA with PBS washing and resuspending, followed by serial extrusion through polycarbonate membrane filters with 5 μ m (3 times) and 0.1 μ m (3 times) pore sizes using an Avanti mini-extruder and filter support. Nanovesicles were collected by centrifugation at $30000 \times g$ for 1 h at 4 °C, followed by quantification using a BCA protein assay kit. Hydrophilic coating was performed by electroporation of nanovesicles (1 mg) and DSPE-PEG (3 mg) using a Neon electroporation system at 1400 V for 2 ms with two pulses, followed by the removal of unreacted DSPE-PEG through tubing dialysis (molecular weight cutoff = 12–14 kDa). Nanovesicles were tagged with fluorescence (DiD) following the manufacturer's instructions. Coating (–) versus (+) nanovesicles (20 μ g in 200 μ L) were injected into the mouse tail vein for in vivo assays.

Splenic CD11b⁺ Cells with Hypoxic Priming: Splenic CD11b⁺ cells were isolated from harvested spleen, using the CD11b selection kit following the supplier's instructions. CD11b⁺ cells were cultured on a plate (3×10^6 cells cm^{–2}) in RPMI 1640 medium supplemented with FBS (10% w/v) and penicillin–streptomycin (1% w/v) in an incubator (5% CO₂, 37 °C). For hypoxic priming, cells were incubated in a hypoxia incubator (1% O₂) or cultured with CoCl₂ (100 μ M) for 72 h with daily medium replenishment. The cells were subjected to optical imaging (Dmi8, Leica Microsystems, Wetzlar, Germany) and PCR, and the results were confirmed by immunofluorescence staining with anti-CD11b (1:200), anti-CD34 (1:200), and anti-SCA1 (1:200), followed by secondary anti-rat Alexa Fluor 594 (1:500) and anti-rabbit Alexa Fluor 488 (1:500). All procedures were described in detail below.

Hemolysis by CoCl₂-coating (+): The hemato-compatibility of CoCl₂-coating (+) was examined by determining the lysis of red blood cells upon incubation. Three test groups [no treat, 42 μ M of CoCl₂-coating (+), and 100 mM CoCl₂ solution (positive control)] were prepared in a buffer solution from the CD11b⁺ selection kit. Each of these test groups (20 μ L) was dropped on a slide glass, followed by adding mouse blood (2 μ L) that was drawn from tail vein. After placing a cover glass to the slide glass, red blood cells were optically imaged at 0, 4, and 24 h with determining the number of lysed cells.

Cell Homing in a 3D Chip: Inflammation-responsive homing of vasculogenic cells after hypoxic reprogramming of splenic CD11b⁺ cells with CoCl₂ was examined on a 3D hydrogel chip with microchannel networks. Tissues were obtained from normal and ischemic hindlimbs of mice using a biopsy punch (1 mm; 69031-01, Integra LifeScience, Princeton, NJ, USA). The cells and tissues were labeled with DiD and DiO, respectively, according to the manufacturer's instructions. A 3D hydrogel chip with a microchannel network was prepared using a custom-made spinning device (2500–2800 rpm) of PNIPAM as sacrificing structural material in methanol (53% w/v), thereby to produce a thread of microvasculature-mimetic fibers as reported previously.^[32] A custom-made mold [7 (width) \times 7 (depth) \times 5 (height) mm] was used to embed PNIPAM fibers (11.45 μ g mm^{–3}), followed by pouring a gelatin solution (5.5% w/v in PBS), inserting the tissues apart to both ends of the chip, and loading vasculogenic cells at the middle of two tissue positions. The chip was incubated at 37 °C for 30 min for gelation by adding microbial transglutaminase (10% w/v in PBS; 1201–50, Modernist Pantry, Eliot, ME, USA). The PNIPAM fibers were removed through the induction of the gel-to-sol transition by washing with PBS (room temperature). The chip was perfused (20 μ L min^{–1}) by placing a 26-gauge needle at the gel center in connection with a syringe pump to flow RPMI 1640 medium with FBS (10% w/v) and penicillin–streptomycin (1% w/v). Tissue viability and vasculogenic cell homing were examined after 24 h of incubation (5% CO₂, 37 °C) using Live & Dead assay kit with confocal microscopy.

In Vitro Effects of Vasculogenic Cells: Proangiogenic effects were examined in transwell inserts (pore size = 0.4 μ m) by co-culturing vasculogenic versus splenic CD11b⁺ cells (upper chamber) with HUVECs (passage 3–6, 5×10^4 per well, Matrigel-coated lower chamber) for 4 h under EGM-2 (Bullet Kit). Tubulogenesis of HUVECs was examined by

optical imaging with angiogenesis analysis using ImageJ (NIH, Bethesda, MD, USA). The results were confirmed by subjecting the supernatant from the upper chamber to VEGF ELISA (900-K10, Peprtech, Cranbury, NJ, USA). For comparison, HUVECs were treated with LPS ($1 \mu\text{g mL}^{-1}$) 24 h before seeding into transwell plates.

Immunofluorescence Staining: In vitro samples were fixed with 4% paraformaldehyde (PFA; CNP015-0500, CellNest, Hanam, Republic of Korea), permeabilized with 0.2% Triton X-100, blocked with 5% BSA, and treated with antibodies. In vivo samples were subjected to paraffin or frozen section as denoted in the corresponding section. Paraffin sections were prepared by fixing samples in 10% neutral-buffered formalin for 24 h, followed by paraffin embedding, and then sectioned at $4 \mu\text{m}$ thickness, deparaffinized, and rehydrated. Frozen sections were prepared by embedding samples in an optimal cutting temperature compound (3801480, Leica Biosystems, Nussloch, Germany), freezing at -80°C , and sectioning to $5 \mu\text{m}$ thickness. The frozen sections were then fixed in 4% PFA for 15 min and permeabilized by blocking with 0.05% Triton X-100 and 1% BSA for 30 min at room temperature.

Next, all samples were treated with primary antibodies overnight at 4°C , washed three times with PBS, and incubated with secondary antibodies for 1 h at room temperature. Confocal microscopy was used for image acquisition, followed by analysis using ZEN software or ImageJ.

Western Blotting: Tissue samples were chopped using surgical scissors or a syringe plunger. Total proteins were extracted using $500 \mu\text{L}$ of RIPA buffer on ice for 2 h, followed by centrifugation at $21000 \times g$ for 30 min at 4°C . Protein content was determined using a BCA protein assay kit, and proteins ($25 \mu\text{g}$) were mixed with $5 \mu\text{L}$ of sample buffer (LI100, GenDEPOT, Katy, TX, USA) and pure water to the final volume of $23 \mu\text{L}$, followed by heating at 95°C for 10 min. Proteins were separated on a 10% SDS-PAGE gel with a protein ladder and then electrotransferred onto nitrocellulose membranes using a gel transfer device. Then, the membranes were blocked with 2.5% skim milk dissolved in (1X) Tris-buffered saline containing 0.5% Tween-20 (TBST; BTT-9110, T&L, Seoul, Republic of Korea) for 1 h at room temperature. Antibodies against CD11b (1:1000) and actin (1:1000; sc-47778, Santa Cruz, Starr Cruz, CA, USA) were diluted with 2.5% skim milk in TBST, and the membranes were incubated with primary antibodies at 4°C overnight, followed by washing with TBST five times (10 min each). The secondary horseradish peroxidase conjugated antibody (1:5000; 31430, Invitrogen) was diluted with 2.5% skim milk in TBST, and the membranes were incubated with secondary antibodies for 1 h at room temperature, followed by washing with TBST five times (10 min each). Band signals were visualized using an enhanced chemiluminescence substrate kit in a biomolecular imager. Data were normalized to the intensity of actin using ImageJ.

PCR: Total RNA was extracted from each sample using TRIzol, and cDNA was synthesized using AccuPower CycleScript RT premix (K2004, Bioneer, Seoul, Republic of Korea) according to the manufacturer's instructions. Real-time PCR was performed using SYBR Green PCR mix with specific primers (Table S1, Supporting Information). Data were normalized to glyceraldehyde 3-phosphate dehydrogenase expression by calculating the $2^{-\Delta\text{Ct}}$ values.

FACS Analysis: Cells were isolated by chopping tissues with surgical scissors or a syringe plunger in a solution of DPBS with 2% FBS. The lysate was then passed through a $70 \mu\text{m}$ strainer and centrifuged at $500 \times g$ for 8 min. The cells were resuspended in a solution of DPBS with 2% FBS and 2 mM EDTA, followed by incubation with antibody for 1 h at 4°C . The cells were subjected to FACS analysis using FlowJo.

Statistical Analysis: Data were presented as mean \pm standard error of the mean (SEM) based on more than three independent experiments, with units of measurement. The sample size for each experiment was denoted in the corresponding legend, and all data were shown (circles, triangles, or squares) in each graph when the sample size was below 10. GraphPad Prism (San Diego, CA, USA) was used for analyses. The significance of differences between two groups was determined using two-tailed Student's *t*-test. Multiple comparisons among the test groups were conducted using one-way analysis of variance (ANOVA), followed by Tukey's post-hoc test. A *p*-value less than 0.05 was considered statistically significant among the groups. The *p*-values were presented

as *, **, and *** for $p < 0.05$, $p < 0.01$, and $p < 0.001$, respectively, with dashed lines between the corresponding groups on each graph.

Supporting Information

Supporting Information is available from the Wiley Online Library or from the author.

Acknowledgements

The present study was supported by Korean government grants, including i) the Korea Medical Device Development Fund grant funded by the Korean Government (Ministry of Science and ICT, Ministry of Trade, Industry and Energy, Ministry of Health & Welfare, and Ministry of Food and Drug Safety) (RS-2020-KD000152), ii) the National Research Foundation (NRF) of Korea Grant funded by the Korean Government (MSIP) (No. NRF-RS-2023-00207857), iii) the Bio & Medical Technology Development Program of the National Research Foundation (NRF) (2020R1C1C1010579-SEY), and iv) the MD-Phd/Medical Scientist Training Program through the Korea Health Industry Development Institute (KHIDI), funded by the Ministry of Health & Welfare, Republic of Korea. The authors thank Medical Illustration & Design, part of the Medical Research Support Services of Yonsei University College of Medicine, for all the artistic support related to this work. The authors acknowledge the support of the Department of Laboratory Animal Resources for pathology, flow cytometry, and electron microscopy.

Conflict of Interest

The authors declare no conflict of interest.

Author Contributions

S.C., S.Y.K., and K.L. contributed equally to this work as co-first authors. S.E.Y. and H.-J.S. (lead) are listed as co-corresponding authors considering their significant contributions. S.C. planned and managed experiments on in situ reprogramming based on nano-hypoxia; in vitro experiments, S.E.Y. and S.P. contributed to data acquisition and analysis; in vivo experiments, H.-S.H. and D.-H.K. conducted mouse surgeries for disease modeling; in ex vivo experiments, S.B. contributed to chip fabrication and data acquisition and analysis. S.Y.K. conducted experiments on splenic targeting of nanoparticles and inflamed skin models with contributions from K.L., C.H.L., and H.-S.K. on data acquisition and analysis. Y.M.S. and H.-J.S. contributed to the study of design. H.-J.S. drafted the manuscript with assistance from S.C., S.Y.K., K.L., and S.E.Y.

Data Availability Statement

The data that support the findings of this study are available from the corresponding author upon reasonable request.

Keywords

angiogenesis, hypoxia, ischemia, nanoparticles, spleen

Received: March 12, 2023

Revised: April 12, 2023

Published online:

- [1] F. K. Swirski, M. Nahrendorf, M. Etzrodt, M. Wildgruber, V. Cortez-Retamozo, P. Panizzi, J. L. Figueiredo, R. H. Kohler, A. Chudnovskiy, P. Waterman, E. Aikawa, T. R. Mempel, P. Libby, R. Weissleder, M. J. Pittet, *Science* **2009**, 325, 612.
- [2] A. J. Mitchell, B. Roediger, W. Weninger, *Cell. Immunol.* **2014**, 291, 22.
- [3] Y. C. Teh, J. L. Ding, L. G. Ng, S. Z. Chong, *Front Immunol* **2019**, 10, 834.
- [4] M. L. Senders, A. E. Meerwaldt, M. M. T. van Leent, B. L. Sanchez-Gaytan, J. C. van de Voort, Y. C. Toner, A. Maier, E. D. Klein, N. A. T. Sullivan, A. M. Sofias, H. Groenen, C. Faries, R. S. Oosterwijk, E. M. van Leeuwen, F. Fay, E. Chepurko, T. Reiner, R. Duivenvoorden, L. Zangi, R. M. Dijkhuizen, S. Hak, F. K. Swirski, M. Nahrendorf, C. Pérez-Medina, A. J. P. Teunissen, Z. A. Fayad, C. Calcagno, G. J. Strijkers, W. J. M. Mulder, *Nat. Nanotechnol.* **2020**, 15, 398.
- [5] S. M. Moghimi, C. J. Porter, I. S. Muir, L. Illum, S. S. Davis, *Biochem. Biophys. Res. Commun.* **1991**, 177, 861.
- [6] A. B. Jindal, *Drug Deliv Transl Res* **2016**, 6, 473.
- [7] J. Hou, X. Yang, S. Li, Z. Cheng, Y. Wang, J. Zhao, C. Zhang, Y. Li, M. Luo, H. Ren, J. Liang, J. Wang, J. Wang, J. Qin, *Sci. Adv.* **2019**, 5, eaau8301.
- [8] J. Che, A. Najer, A. K. Blakney, P. F. McKay, M. Bellahcene, C. W. Winter, A. Sintou, J. Tang, T. J. Keane, M. D. Schneider, R. J. Shattock, S. Sattler, M. M. Stevens, *Adv. Mater.* **2020**, 32, 2003598.
- [9] T. Asahara, T. Murohara, A. Sullivan, M. Silver, R. van der Zee, T. Li, B. Witzendichler, G. Schatteman, J. M. Isner, *Science* **1997**, 275, 964.
- [10] C. Kalka, H. Masuda, T. Takahashi, W. M. Kalka-Moll, M. Silver, M. Kearney, T. Li, J. M. Isner, T. Asahara, *Proc Natl Acad Sci USA* **2000**, 97, 3422.
- [11] H. Kamihata, H. Matsubara, T. Nishiue, S. Fujiyama, Y. Tsutsumi, R. Ozono, H. Masaki, Y. Mori, O. Iba, E. Tateishi, A. Kosaki, S. Shintani, T. Murohara, T. Imaizumi, T. Iwasaka, *Circulation* **2001**, 104, 1046.
- [12] N. Werner, S. Junk, U. Laufs, A. Link, K. Walenta, M. Bohm, G. Nickenig, *Circ. Res.* **2003**, 93, e17.
- [13] V. Schächinger, S. Erbs, A. Elsässer, W. Haberbosch, R. Hambrecht, H. Hölschermann, J. Yu, R. Corti, D. G. Mathey, C. W. Hamm, T. Süselbeck, B. Assmus, T. Tonn, S. Dimmeler, A. M. Zeiher, *N. Engl. J. Med.* **2006**, 355, 1210.
- [14] M. Tendera, W. Wojakowski, W. Ruzyło, L. Chojnowska, C. Kepka, W. Tracz, P. Musiałek, W. Piwowarska, J. Nessler, P. Buszman, S. Grajek, P. Breborowicz, M. Majka, M. Z. Ratajczak, *Eur. Heart J.* **2009**, 30, 1313.
- [15] A. A. Quyyumi, E. K. Waller, J. Murrow, F. Esteves, J. Galt, J. Oshinski, S. Lerakis, S. Sher, D. Vaughan, E. Perin, J. Willerson, D. Kereiakes, B. J. Gersh, D. Gregory, A. Werner, T. Moss, W. S. Chan, R. Preti, A. L. Pecora, *Am Heart J* **2011**, 161, 98.
- [16] J. Hoover-Plow, Y. Gong, *Vasc Health Risk Manag* **2012**, 8, 99.
- [17] M. R. Hoenig, C. Bianchi, F. W. Sellke, *Curr. Drug Targets* **2008**, 9, 422.
- [18] S. W. Lee, H. K. Jeong, J. Y. Lee, J. Yang, E. J. Lee, S. Y. Kim, S. W. Youn, J. Lee, W. J. Kim, K. W. Kim, J. M. Lim, J. W. Park, Y. B. Park, H. S. Kim, *EMBO Mol. Med.* **2012**, 4, 924.
- [19] C. Liu, A. L. Tsai, P. C. Li, C. W. Huang, C. C. Wu, *Stem Cell Res Ther* **2017**, 8, 29.
- [20] S. Y. Choo, S. H. Yoon, D. J. Lee, S. H. Lee, K. Li, I. H. Koo, W. Lee, S. C. Bae, Y. M. Lee, *Int J Oncol* **2019**, 54, 1327.
- [21] C. W. Pugh, P. J. Ratcliffe, *Nat. Med.* **2003**, 9, 677.
- [22] A. Weidemann, R. S. Johnson, *Cell Death Differ.* **2008**, 15, 621.
- [23] H. Rinderknecht, S. Ehner, B. Braun, T. Histing, A. K. Nussler, C. Linnemann, *Oxygen* **2021**, 1, 46.
- [24] Z. Wang, Z. Chen, Q. Zuo, F. Song, D. Wu, W. Cheng, W. Fan, *J Orthop Sci* **2013**, 18, 388.
- [25] R. Wan, Y. Mo, Z. Zhang, M. Jiang, S. Tang, Q. Zhang, *Part. Fibre Toxicol.* **2017**, 14, 38.
- [26] F. Zheng, Z. Luo, C. Zheng, J. Li, J. Zeng, H. Yang, J. Chen, Y. Jin, M. Aschner, S. Wu, Q. Zhang, H. Li, *Toxicol. Appl. Pharmacol.* **2019**, 369, 90.
- [27] S. L. Groenland, R. H. J. Mathijssen, J. H. Beijnen, A. D. R. Huitema, N. Steeghs, *Eur J Clin Pharmacol* **2019**, 75, 1309.
- [28] J. W. Lee, J. Ko, C. Ju, H. K. Eltzschig, *Exp. Mol. Med.* **2019**, 51, 68.
- [29] M. Hölscher, K. Schäfer, S. Krull, K. Farhat, A. Hesse, M. Silter, Y. Lin, B. J. Pichler, P. Thistlethwaite, A. El-Armouche, L. S. Maier, D. M. Katschinski, A. Zieseniss, *Cardiovasc. Res.* **2012**, 94, 77.
- [30] J. C. Stewart, *Anal. Biochem.* **1980**, 104, 10.
- [31] C. Mitchell, H. Willenbring, *Nat. Protoc.* **2008**, 3, 1167.
- [32] S. J. Yoon, S. Baek, S. E. Yu, E. Jo, D. Lee, J. K. Shim, R. J. Choi, J. Park, J. H. Moon, E. H. Kim, J. H. Chang, J. B. Lee, J. S. Park, H. J. Sung, S. G. Kang, *Adv. Healthcare Mater.* **2022**, 11, 2201586.